Effect of raindrop splash and transversal width on soil erosion: Laboratory flume experiments and analysis with the Hairsine-Rose model

S. Jomaa [a,*], D.A. Barry [a], A. Brovelli [a], G.C. Sander [b], J.-Y. Parlange [c], B.C.P. Heng [b,1], H.J. Tromp-van Meerveld [d]

[a] *Laboratoire de technologie écologique, Institut d'ingénierie de l'environnement, Station 2, Ecole polytechnique fédérale de Lausanne (EPFL), CH-1015 Lausanne, Switzerland*. Ph. +41 (21) 693-8073; +41 (21) 693-5576; +41 (21) 693-5919; Fax. +41 (21) 693-8035. E-mail addresses: seifeddine.jomaa@epfl.ch, andrew.barry@epfl.ch, alessandro.brovelli@epfl.ch

[b] *Department of Civil and Building Engineering, Loughborough University, Loughborough LE11 3TU United Kingdom*. Ph. +44 (1509) 223-777; Fax. +44 (1509) 223-981; Ph. +1 (520) 626-3251; Fax. +1 (520) 621-2672. E-mail addresses: g.sander@lboro.ac.uk, bcpheng@email.arizona.edu

[c] *Department of Biological and Environmental Engineering, Cornell University, Ithaca, New York 14853-5701 USA*. Ph. +1 (607) 255-2476; Fax. +1 (607) 255-4080. E-mail address: jp58@cornell.edu

[d] *Department of Geography, Simon Fraser University, Burnaby, British Columbia, BC V5A 1S6 Canada*. Ph. +1 (778) 782-3386; Fax. +1 (778) 782-5841. E-mail address: ilja@sfu.ca

Re-submitted to *Journal of Hydrology*, 17 September 2010, Accepted 12 October 2010

* Author to whom all correspondence should be addressed

[1] Now at: Department of Geosciences, University of Arizona, Tucson, Arizona 85721 USA

Abstract

The parameter consistency of the one-dimensional Hairsine-Rose (H-R) erosion model under conditions of significant rainfall splash was examined. To account for the splash characteristic length scale and its interaction with the transverse erosion width, experiments were carried out using erosion flumes of the same length (6 m), but different widths, with sediment concentrations measured at the flume exits. Total sediment concentration and the concentration of seven size fractions (< 2, 2-20, 20-50, 50-100, 100-315, 315-1000 and > 1000 μm) were measured at high rainfall intensity (60 mm h^{-1}) and with a gentle slope (2.2%). The conditions employed ensured that erosion was predominantly precipitation-driven. The experimental results showed that raindrop splash affected particularly the sediment breakthrough from the wider flumes (flumes 1 and 2, 1- and 0.5-m wide, respectively). However, the raindrop splash effect was less significant in observed sediment concentrations from the narrower flumes (flumes 3 and 4, both 0.25-m wide). For these flumes, the detached sediment was affected by the transversal width of the flume in that an amount of detached sediment adhered to the barriers instead of being removed in the overland flow. The one-dimensional H-R model was fitted to the experimental results and good agreement was found, in particular for the finer size classes. The data for the coarser grain sizes were more scattered, suggesting sediment motion by mechanisms other than as a suspension in the overland flow (e.g., rolling along the soil surface). The optimized parameters indicated that the shield layers (where the shield consists of redeposited eroded sediment) of the wider flumes (1 and 2) developed within 5-10 min from the start of the experiment, whereas in the narrower flumes (3 and 4) they never fully developed. The optimized detachment rates were consistent with previous findings, but the estimated thickness of the deposited layer was too small to provide complete protection of the original soil against raindrop detachment, indicating

that the shield was not uniform. The experimental design allowed us to investigate directly the effect of flow non-uniformity on soil erosion by inclusion of an offset drainage point in flume 4. The observations taken during and after the experiment, as well as surface elevation data, confirmed the noticeable impact of non-uniform flow on the erosion process.

Keywords: Interrill erosion, Sediment concentration, Digital terrain model (DTM), Erosion flume, Transverse width, Boundary condition asymmetry, Rainfall splash

1. Introduction

Soil erosion as a result of rainfall and overland flow is a serious environmental problem involving different complex processes that drive sediment transport. Soil loss and its associated impacts affect agricultural productivity, the natural environment and infrastructure security. Factors influencing sediment transport include rainfall intensity, soil properties, topography, land cover, antecedent conditions and spatial scale (Rudolph et al., 1997; Römkens et al., 2002; Gomez et al., 2003; Hancock et al., 2008). Despite the complexities involved, process-based erosion modeling has proven to be a useful tool for the description and prediction of soil erosion and sediment transport.

Process-based erosion models are used to forecast the spatial and temporal variation of transported suspended sediments. Among the available simulators, the 1D Hairsine-Rose (hereafter H-R) erosion model (Rose et al., 1983a,b; Hairsine and Rose, 1991; 1992a,b) describes time-varying suspended sediment concentrations of multiple particle sizes, and accounts for key soil erosion mechanisms: rainfall detachment, overland-flow entrainment and gravity deposition. The H-R model, in contrast to most of the other process-based erosion models, considers erosion and deposition processes separately and accounts for the contributions of each particle size class to the total sediment concentration. The latter is an important feature of H-R model, since sediment erosion, transport and deposition rates are strongly dependent on the particle size.

Rainfall simulators have shown to be beneficial tools for studying the effect of different soil variables and environmental conditions (such as slope, initial moisture content, surface soil coverage, initial roughness, rain intensity, etc.) on soil erosion processes and sediment transport at different scales. In particular, rainfall simulators are useful to gain insights into the soil erosion

mechanisms and to develop and validate process-based erosion models. The 1D H-R model has been evaluated with rainfall simulations experiments under different experimental configurations and soil types, and has been shown to explain experimental data in a consistent manner (Proffitt et al., 1991; Sander et al., 1996; Heilig et al., 2001; Gao et al., 2003; Walker et al., 2007; Tromp-van Meerveld et al., 2008; Heng et al., 2009).

The H-R model has not been validated under conditions leading to significant raindrop splash even though this mechanism might be very important in some circumstances, e.g., interrill erosion (Planchon et al., 2000; van Dijk et al., 2002; Leguedois et al., 2005). Leguedois and Le Bissonnais (2004) and Leguedois et al. (2005) defined the splash impact as a process that acts to move the soil particles from their original position (detachment). Rainfall-induced splash displacement depends on several factors including rainfall intensity, raindrop characteristics (fall velocity, drop size distribution), soil properties (cohesion, initial water content, surface compaction and roughness) and local flow patterns (Planchon et al., 2000). Ideal conditions for raindrop-driven erosion include a dry and completely disaggregated soil, high rainfall intensity, gentle slope and absence of upstream flow (Planchon et al., 2000; Salles and Poesen, 2000; Mouzai and Bouhadef, 2003). Legout et al. (2005a,b) showed experimentally that soil particles/fragments up to a size of 2000 µm can be transported by raindrop impact.

Depending on their characteristics (e.g., settling velocity) and ambient flow conditions (e.g., flow rate and depth), the particles can either return to the bed or be transported considerable distances by the overland flow and be effectively removed from the soil under consideration, i.e., they are eroded.

After erosion is initiated, the suspended and redeposited soil particles form a shield layer. Proffitt et al. (1991) and Sander et al. (1996) pointed out that when the overland flow depth is around three times greater than raindrop diameter, the rainfall detachability of both the original soil and the deposited shield layer decreases considerably. Under these circumstances, raindrop splash affects the short time behavior much more than long time behavior.

Van Dijk et al. (2002) and Leguedois et al. (2005) studied the splash-induced distribution of different size soil particles for aggregated soils and found that the average splash distance ranged from 4 to 23 cm, independent of the soil type. In addition, they found that the greatest splash-induced displacements were for the mid-size fractions (100-200 μm).

In any 1D erosion model there is a transverse (perpendicular to flow) distance over which the erosion and flow processes are averaged. It is not known at present whether, in an experiment, the size of the averaging width affects the measured results. Rainfall splash, which has a characteristic length scale for given rainfall and soil conditions, potentially provides an additional transport mechanism. The possible interaction of this length scale and the transverse averaging width has yet to be investigated.

The aim of this study was to conduct a suite of experiments to analyze the effect of raindrop splash erosion and transversal (to flow direction) width on soil erosion, and to evaluate whether the 1D H-R model can reproduce the observed behavior. The initial soil conditions (cohesiveness, roughness and moisture content) and the rainfall intensity were chosen to generate raindrop splash at the commencement of the erosion event. The effect of the splash and transverse length scale were ascertained by carrying out experiments with identical initial conditions (soil surface and hydrology) but on erosion flumes having different transversal widths

and position of the sediment collector. The comparison between experimental results and model predictions provides the basis upon which to investigate parameter consistency in the H-R model for erosion situations where raindrop splash is significant and the transverse width is comparable to the characteristic length scale of the splash.

2. Methods

2.1. Experimental setup

The erosion experiments were performed at the erosion flume of the Ecole Polytechnique Fédérale de Lausanne (EPFL), Switzerland (Fig. 1), which includes a rainfall simulator (Viani, 1986; Baril, 1991; Tromp-van Meerveld et al., 2008). In the following, only the major components of the apparatus are presented, as well as the principal modifications that were implemented for this study.

Figure 1 near here

The flume is equipped with a hydraulic slope control device and a sprinkling system that provides a near-uniform spatial rainfall distribution (Viani, 1986; Tromp-van Meerveld et al., 2008). The EPFL flume is filled to a depth of 0.32 m with an agricultural loam (35% sand, 31% silt, 22% clay, 12% fine gravel) from Sullens (Canton Vaud, Switzerland). The soil's particle size distribution is shown in Fig. 2.

Figure 2 near here

The flume was subdivided into four smaller sections for the purpose of investigating the interaction between the characteristic rainfall splash distance and the transverse averaging width inherent in application of the H-R model. The largest characteristic distance for raindrop-induced

splash is around 0.23 m (Leguedois et al., 2005). On the assumption that most splashes will be much shorter than 0.23 m, we a priori assumed 0.25 m as the minimum distance over which transverse averaging of the H-R model was reasonable. Visual observations during the experiments confirmed that 0.25 m is about 5-10 times the typical raindrop splash disturbance length scale. The flume was divided into four smaller flumes, with widths 1 m, 0.5 m and 2 × 0.25 m (flumes 1-4 respectively), but otherwise prepared so as to be identical (Fig. 3). Splash in the smallest flumes (3 and 4) has the potential to interact markedly with the vertical barriers separating each flume. In flumes 1-3 the water/sediment collection point was centrally located, as indicated in Fig. 3. For these three flumes, the sediment concentration in the collected samples was a realistic average value over the cross-section. In flume 4 the water-sediment collection point was offset. Here, the goal was to evaluate the effect of this boundary condition asymmetry on the experimental data and, in a subsequent step, on the parameters deduced from the H-R model.

Figure 3 near here

A key element in the experimental design was to ensure, as far as possible, that each flume was an experimental replicate, except for the differences already described. The main variables are (i) the precipitation uniformity, (ii) the initial moisture content and (iii) the initial condition of the erodible soil, especially slope and surface roughness. Precipitation was applied to the flume with 10 Veejet nozzles located on two parallel oscillating bars 3 m above the soil surface using water from Lake Geneva. The average rainfall intensity was adjusted by changing the oscillation frequency of the sprinklers, i.e., at higher oscillation frequencies the rainfall rate increases because the water supplied during one oscillation cycle is constant. Tromp-van Meerveld et al. (2008) tested the spatial distribution of the rainfall system over the flume and

found that the precipitation was near uniform with a uniformity coefficient (Christiansen, 1942) of 0.86. Before the present experiments were conducted, the rainfall uniformity was again checked and similar results were obtained. Since the experiment was designed to investigate raindrop-induced splash, dry (initial moisture content ≈ 5%) and disaggregated soil exposed to high rainfall intensity (60 mm h^{-1}) on a gentle 2.2% slope was used. The initial moisture content was determined using 5TE probes (Decagon, Hopkins, USA, http://www.decagon.com). These conditions are ideal to generate raindrop splashes at the commencement of the erosion event (Salles and Poesen, 2000; Mouzai and Bouhadef, 2003), and ensure that the duration of the effect would be controlled by the buildup of water on the soil surface, so that the transient nature of the splash effect could be observed.

Before the experiment, the top 0.2 m of the soil surface was re-ploughed and gravel (> 20 mm on the longest axis) removed. Then, the soil surface was smoothed using a mechanical system that ensured, within practicality, a consistency smooth surface. The preparation method was such that the initial dry bulk density of the surface soil was relatively low, measured to be about 1118 ± 20 kg m^{-3}. After the experiment, the dried soil formed a crust of about 10-mm thickness. Both sediment concentrations and overland flow rate were measured as a function of time for each collector shown in Fig. 3. In order to get a single value for flume 2, the sediment concentrations measured from collector 3b.1 and 3b.2 were averaged. A summary of the experimental conditions is given in Table 1.

The samples from the collectors in Fig. 3 were in individual 0.5-l increments (in sample bottles). Continuous sampling took place for the first 30 min of the experiment. Afterwards, samples were collected every 5, 10 or 15 min, with the sampling period increasing towards the end of the experiment. The experiment duration was 160 min. For each sample, the time needed

to fill the sample bottle was recorded and used to deduce the overland flow rate as a function of time. For each bottle, the total sediment concentration and the size class distribution were measured using sieving and laser diffraction granulometry. Sieving was used to determine the mass of the three largest classes (> 2000 μm, 315-1000 μm and 100-315 μm) in each sample. Then the volume of the remaining four finer fractions (< 2 μm, 2-20 μm, 20-50 μm and 50-100 μm) was measured using a laser granulometer. Subsequently, the sample bottles were left until the water was clear, at which time the samples were oven-dried to obtain the total mass and the mass for each size class.

Table 1 near here

2.2. Digital terrain models (DTM)

It is common to apply 1D (i.e., longitudinal) erosion models even though the overland flow and sediment transport processes should be considered two- (longitudinal and transverse) or three-dimensional (longitudinal, transverse and depth), depending on the level of detail desired. One-dimensional parameter determinations, which are based typically on outflow data, implicitly average the flow. To understand better whether sediment transport during the erosive events should be modeled as a 2D process, an investigation of the initial surface roughness and its evolution over the course of the experiment has been recommended (Hancock et al., 2008). Moreover, there is a large body of literature dealing with the question of the initial surface roughness and its effect on sediment transport predictions (Johnson et al., 1979; Cogo et al., 1983; Onstad et al., 1984; Bertuzzi et al., 1990; Gomez et al., 2003; Darboux and Huang, 2005; Gomez and Nearing, 2005; Le Bissonnais et al., 2005). For instance, excessive soil surface roughness and non-uniformity leads to local barriers that form surface pools that have the potential to affect the sediment concentration as it varies temporally and spatially.

The methods used to measure surface elevations include digital photogrammetry, motorized total stations, LIDAR and laser-scanning (Römkens and Wang, 1987; Bertuzzi et al., 1990; Darboux and Huang, 2003; Rieke-Zapp and Nearing, 2005; Hancock et al., 2008). Recently, Hancock et al. (2008) have shown the ability of laser scanners to provide accurate spatial data. Accordingly, to better understand the change in surface elevation and to identify whether surface non-uniformity has had an impact, laser scanning of the soil surface was carried out before and after the experiment and digital terrain models (DTM's) were created and compared.

The soil surface DTM's measured before and after the experiment are shown in Fig 4. The acquisitions were performed using a FARO Laser Scanner (http://laser-scanner.faro.com). The scanner used had vertical and horizontal angular resolutions of 9×10^{-3}° and 7.6×10^{-4}°, respectively, which resulted in a theoretical spatial resolution of less than 1 mm. While this may have been a reasonable precision in the interior of the flume, near the edges it was found that the results were inconsistent with visual observations. The raw data were processed to allow a quantitative direct comparison. In particular, the effect of the slope was removed from the images and the same reference point was set for both scans using a known location on the flume.

Figure 4 near here

2.3. Modeling

2.3.1. Governing equations

Hairsine and Rose (1991) developed a soil erosion model that describes erosion transport for rainfall-impacted flows in the absence of entrainment by overland flow. Entrainment occurs when the stream power, Ω, exceeds a threshold value, Ω_{cr}, appropriate for the soil investigated. Beuselinck et al. (2002) analyzed the experimental data of a loamy Belgian soil, and estimated

Ω_{cr} to be 0.15 – 0.20 W m^{-2}, which we take as a typical range. For the experiments reported here, Ω was estimated as (Beuselinck et al., 1999a):

$$\Omega \approx \rho g q S \approx 0.003 \text{ W m}^{-2}, \quad (1)$$

where ρ is water density (1000 kg m^{-3}), g is the magnitude of gravitational acceleration (9.81 m s^{-2}), q is the volumetric flux per unit width, $q \approx (P - I)L = 1.33 \times 10^{-5}$ m^2 s^{-1}, with P and I the precipitation and infiltration rates, L and S the flume width and slope, respectively. The value of Ω estimated from Eq. (1) is much smaller than the threshold value Ω_{cr}. It was therefore concluded that entrainment can be ignored in the experiments considered here. Rill formation was not observed during the experiment and was not evident in the DTM data either (Fig. 4), suggesting that the rill erosion did not occur and that rainfall splash soil erosion was the dominant erosion mechanism.

The governing equations of H-R erosion model have been described in detail elsewhere (Hairsine and Rose, 1991; Sander et al., 1996; Lisle et al., 1998; Parlange et al., 1999; Sander et al., 2007; Tromp-van Meerveld et al., 2008; Heng et al., 2009; Barry et al., 2010), so only a brief summary is given here. From conservation of mass of both the suspended sediment and the sediment in the deposited layer for size class i the H-R model is given by:

$$\frac{\partial (D c_i)}{\partial t} + \frac{\partial (q c_i)}{\partial x} = e_i + e_{ri} - d_i, \quad (2)$$

and

$$\frac{\partial m_i}{\partial t} = d_i - e_{ri}, \quad (3)$$

where x is the downslope distance, D is flow depth, c_i is the suspended sediment concentration and m_i is the deposited sediment mass per unit area for sediment size class i. The source/sink

terms e_i, e_{ri} and d_i are, respectively, the detachment and re-detachment rates due to rainfall and the rate of deposition with units of mass per unit area per unit time. The rates of rainfall detachment from the original soil and from the deposited layer are evaluated as:

$$e_i = (1-H)\, p_i a P, \tag{4}$$

and

$$e_{ri} = H \frac{m_i}{m_t} a_d P, \tag{5}$$

where a is the detachability of the original soil, and a_d is the detachability of the deposited layer in mass per unit area per unit flow depth, p_i is the proportion of class i sediment in the original soil, $m_t = \sum m_i$ is the total deposited sediment mass per unit area, H = min (m_t/m_t^*,1) represents the degree of shielding provided by deposited sediment, and m_t^* is the mass of deposited sediment required to shield the original soil completely. The rate of deposition for sediment class i is given by $d_i = v_i c_i$, where v_i is the settling velocity of particles in that class. Fig. 5 illustrates the different compartments of the HR erosion model along with the physical processes.

Figure 5 near here

Sander et al. (1996) presented an approximate analytical solution to the above model that agrees well with experimental data obtained from the nine experiments of Proffitt et al. (1991); their solution is used in the data analysis below. The analytical solution was derived assuming that the transport of water and sediments occur in a uniform strip and is shallow enough for the kinetic overland flow approximation to be valid. Additionally, the solution ignores the initial transient hydrological effects on the concentrations. In other words, this assumption means that for limited slopes and water flow velocities the sediment concentration is fairly uniform in space

and that during the erosion event the variations in time of the concentrations near the collector are greater than the spatial variability, i.e., $\frac{\partial(Dc_i)}{\partial t} >> \frac{\partial(qc_i)}{\partial x}$. Furthermore, Sander et al. (1996) assumed that the overland flow depth, *D*, remains constant in space and time. As discussed by Sander et al. (1996) and Tromp-van Meerveld et al. (2008), this simplification is reasonable if the topography is regular, the rainfall rate is homogeneous, and the initial phase of the experiment, when irregular hydrologic behavior occurs, is discarded. According to Proffitt et al. (1991), water flow reaches the steady state very quickly (1 min or less), a time scale that is negligible compared to the duration of the experiment. In our experimental results (reported below), the observed short-time behavior affects the sediment concentration initial condition, as discussed below.

2.3.2. Model application

An important and unique feature of the H-R model is that the soil is divided into different classes. Seven size classes were identified with different mass proportions (Table 2) according to the grain size distribution. At the commencement of the experiment, runoff did not occur due to the initially high infiltration rate in the dry soil. Afterwards the surface layer became fully saturated and runoff started. The time-to-runoff is about 7 min after the start of the precipitation. As soon as overland flow first reached the downstream collector, the material detached by raindrop splash that had accumulated over the flume produced high sediment concentrations in the early stages of the experiment (0-20 min). The model initial conditions were therefore set to match the short-time behavior observed in the experiment and, to this end, the initial measured sediment concentrations were used to define the initial mass of each granulometric class.

Settling velocity is an important parameter for the prediction of soil erosion concentrations. Tromp-van Meerveld et al. (2008) used the same soil as in this study and determined the settling velocities of the seven sediment classes. For the three finer classes (< 2, 2-20 and 20-50 μm) Stokes' law was used (Stokes, 1851), whereas for the remainder (50-100, 100-315, 315-1000 μm) settling velocities were estimated using a 0.47-m long tube filled with tap water. The estimated range of the settling velocities as well as the values used, are reported in Table 2 and corresponds to the observed settling velocities of Tromp-van Meerveld et al. (2008).

Sander et al.'s (1996) analytical solution assumes steady overland flow and to calculate this value for all the experiments presented in this work the following procedure was used: The infiltration rate (I) was calculated as the difference between the rainfall intensity (P) and the steady state excess rainfall rate (R),

$$I = P - R. \quad (6)$$

At the commencement of each experiment the soil was dry and as rainfall started the infiltrating water progressively increased the soil water content until saturation, when overland flow occurred. According to the measurements, and due to the soil surface roughness, it took about 20 min to reach steady state discharge. The fluxes per unit widths were calculated based on the measured discharge of all flumes. Results indicate that the four flumes discharged the same amount of water per unit width. For flume 1 (width of 1 m) the calculated discharge Q was 80 $cm^3\ s^{-1}$ and consequently the flux per unit width, q, was equal to 0.8 $cm^2\ s^{-1}$. Using the kinetic approximation for the steady state discharge of the flume, $q = Rl$ (l is the length of the flume, here equal to 6 m) the steady state excess rainfall rate R is 48 mm h^{-1} and using Eq. (6) the infiltration rate I is 12 mm h^{-1}.

309 Table 2 near here

310 2.3.3. Parameter estimation

311 Although some model inputs were independently estimated or measured (e.g., fraction of each
312 sediment class, overland flow depth, settling velocities, etc.), some of the parameters had to be
313 estimated to fit the model on the experimental data. Initially, a trial-and-error procedure was used
314 to identify the most influential parameters, and to evaluate whether the data could be fitted using
315 realistic values. In particular, three parameters; the detachability of the original soil, a, the
316 detachability of the shield layer, a_d, and the mass required to complete the shield layer, m_t^*, were
317 analyzed. To optimize manually the parameters, initially the long-time soil erosion behavior was
318 fitted (steady state). To this end a_d was adjusted until a reasonable fit of the steady state behavior
319 of the total and individual size classes' concentration was obtained. Next, the short time sediment
320 concentrations were fitted (value of the peak and its subsequent decline). This involved
321 simultaneous adjustment of a and m_t^*.

322 As a second step an automated procedure was implemented to perform a better calibration.
323 The procedure is a combined global/local approach, used successfully elsewhere (e.g.,
324 Bajracharya and Barry, 1995): (i) For each parameter, a physical sensible range was defined
325 based on literature values (ii) the parameter space was sampled using a Latin hypercube search
326 method to identify a number of initial guesses for the subsequent (iii) minimization of a least-
327 squares objective function. For (iii), a downhill minimization algorithm was used, based on the
328 derivative-free simplex search method. The optimal parameter set was selected considering two
329 metrics, i.e., the highest correlation coefficient and the lowest residual error. In the third step, the
330 settling velocities of some sediment size classes were also adjusted, and the same procedure
331 repeated to evaluate the importance of these values.

3. Results

3.1. Erosion experiments

3.1.1. Sediment breakthrough of flumes 1 (1-m wide) and 2 (0.5-m wide)

The effluent sediment concentrations measured in flumes 1 and 2 are presented in Figs. 6 and 7, respectively. The two flumes showed consistent behavior. A short time peak is visible in the total sediment concentration and in the breakthrough curves of nearly all the individual size classes except for the coarser class (> 1000 µm) of flume 1 and the 20-50 µm class of flume 2. For both flumes, the short-time peaks were more pronounced for the finer particles, i.e., size classes < 2, 2-20 µm. Mid-size classes (20-50 and 50-100 µm) instead showed a more attenuated – even negligible – response with a less pronounced peak. For the larger particles (100-315 and 315-1000 µm) both flumes showed also a short time response, although this was less pronounced for flume 2. This suggests that particles belonging to these classes behaved similarly to the finer particles and thus contributed to the short-time total sediment concentrations. In other words, the results of these two flumes suggest that also the coarser particles were affected by the raindrop splash. There are at least two possible explanations for the different amplitude of the peak in flume 2 (with smaller width): (i) the initial roughness of the soil was not the same for flumes 1 and 2. Larger particles, which are suspended and re-deposited with a higher frequency than smaller particles due to their higher settling velocity, are more sensitive than finer particles to the soil roughness. (ii) Since flume 2 was narrower than flume 1 the effect of the boundaries on the splash might be more pronounced, thus reducing the effect of raindrop splash. The hypothesis of different initial soil roughness was to some extent supported by the visual comparison of the soil surface using the DTM before the experiment. Finally, the data for the coarser class (> 1000 µm) showed a very high level of scatter. This may possibly be due to the stochastic nature of raindrop

and splash transport, especially near the end of the flume, resulting in episodic ejections of larger particles off the flume.

It has been reported that at the beginning of an erosive event most of the contribution to the total suspended sediment concentration comes from the finer particles and only at later times does the contribution of the larger particles to the total sediment behavior become significant (Proffitt et al., 1991). Here, however, at the commencement of the experiment the contribution of the larger particles was present as well as the finer particles. This is likely due to the experimental method whereby the soil was prepared and then the rainfall was initiated. The initial part of the flow reaching the end of the flume would thus have contained detached particles of all class sizes. As mentioned already above, it seems that the initial conditions play a crucial role to determining the contributions of the different particles to the total sediment concentrations.

Figures 6 and 7 near here

Over the course of the experiment, generally speaking the sediment concentrations displayed an initial transient period characterized by rapid changes that diminished after about 25 min. This was followed by a slower change until, at around 160 min, for most size classes a stable long-time sediment concentration was reached. These long time concentrations resemble the composition of the original soil in the erosion flume (Figs. 6 and 7) as predicted by the H-R theory (Parlange et al., 1999).

3.1.2. Sediment breakthrough of flume 3 (0.25-m wide)

Flume 3 was characterized by a small width and by the central position of the drainage collector at the downstream end of the flume. The measured breakthrough curves for this flume

are depicted in Fig. 8. At the beginning of the soil erosion event, the largest contribution to the total sediment concentration was from smaller particles (< 2 and 2-20 μm). In addition, the sum of the sediment concentrations of the smallest size fractions increased quickly from the commencement of runoff until the peak total sediment concentration was reached. However, as previously observed (Proffitt et al., 1991), at later times, when most of the finer particles were suspended and removed, the contribution of the larger particles to the total sediment concentration (100-315 μm, 315-1000 and < 1000 μm) increased gradually. This behavior reflects the development of the deposited layer, which is quantified by *H* (Eqs. 4 and 5). As this layer grows *H* increases and there is reduced access to the original soil. Consequently, the initial peak, which arises from the uniform detachment at early times when *H* is very small, cannot be maintained as *H* grows. Since at steady state *H* is less than unity, detachment of small particles from the original soil is still occurring, maintaining the contribution of the finer particles.

Figure 8 near here

The midsize fractions (diameter > 50 μm) instead did not show the sharp concentration increase at early time observed for the fine materials. This suggests that mid- and coarse-particles are nearly unaffected by raindrop splash if the flume is narrow, or that the flume walls have limited their movement. This is consistent with the observations made for flumes 1 and 2 regarding the short-time behavior of the coarser classes. In other words, the results of the experiments consistently suggest that as the width of the flume is reduced, the initial mobility of the coarser particles due to raindrop splash is reduced. Visual observations confirmed that the transversal barriers (elevation of 0.1 m) were high enough to confine the majority of the splash within the flume. It was however observed that the mass accumulated near or on the solid boundaries of the flumes steadily increased from flumes 1 to 3. The material attached to the

barrier was quantified following the experiment (Table 1). It belongs mainly to the mid-size classes, as can be deduced from Fig. 2. Images of the soil surface taken before and after the experiment confirmed that some material accumulated near the walls probably because (i) the coarser soil particles detached by the splashes hit the wall, then bounced back and landed next to the barriers, (ii) the water flow velocity was locally smaller thus decreasing the mobility of particles with higher settling velocity, and (iii) the shadow effect of the barriers, i.e., less rainfall reached the soil close to the walls. It is therefore likely that initially the coarser particles accumulated next to the boundaries and did not move downstream.

3.1.3. Sediment breakthrough of flume 4 (0.25-m wide)

Flume 4 had a configuration similar to flume 3 except that the drainage point was offset (Fig. 3). The system was designed to check the effect of the asymmetry on sediment transport and to determine the applicability of the H-R model for this situation.

Figure 9 near here

Discharged sediment concentrations are shown in Fig. 9. An early peak was observed for the finer particles (< 2 and 2-20 μm) similar to the three other flumes. The peak was less pronounced for the mid-size classes (20-50 and 50-100 μm) but was again clearly visible for the larger size fractions (100-315 and 315-1000 μm). Once again, the observations for the larger particles (> 1000 μm) showed some scatter in the data and it was difficult to identify any clear pattern. Even though flumes 3 and 4 are the same size, the concentrations of the large particle size classes did not show a consistent trend, whereas for the fine and mid-size the behavior of the two flumes was comparable. In particular, the breakthrough of the 100-315 μm sediments of flume 4 was consistently smaller than the sediment concentrations for the corresponding class in flume 3. A similar behavior was observed for the 315-1000 μm size class but, additionally, in flume 4 a

sharp increase of the sediment concentration was measured that reached a maximum about 10 min after the commencement of runoff and disappeared within the subsequent 10 min. It was then concluded that the position of the water and sediment collector affected only the concentration of the coarser particles, while the fine and mid-size classes were not significantly modified. Visual inspection demonstrated that the location of the discharge pipe affected the symmetry of the flow field near the downstream end of the flume. This can be seen in the DTM after the erosion experiment (right panel of Fig. 4). In the left-lower corner a region with slightly higher elevation is present. Since the collector of flume 4 was located at the same end, but opposite corner, it was concluded that on the left side the flow velocity was significantly reduced, and the heavier particles were able to settle. This conclusion was further corroborated by the granulometric analysis of the sediment deposited near the left corner of flume 4. The measurements are reported in Fig. 2 where it is evident that the relative amount of the fine fractions was significantly reduced, whereas the three coarser fractions were enriched compared of the original soil.

3.1.4. Eroded soil mass and elevation changes

From the comparison of the surface scans acquired before and after the erosion event it was found that the elevation of the soil surface was reduced on average by 2.5 cm, with a range of 1.5-3 cm. Furthermore, the DTM after the erosion experiments showed four lines perpendicular to the flume's slope. These roughly parallel depressions were at distances 0.5, 2, 3.5, and 5 m from the bottom of the flume. As these four regions occurred half way between the five pairs of sprinklers (Fig. 1), it is likely that the zones with greater erosion are due to the increased precipitation rate – and detachment rate – resulting from the overlapping sprinklers. Observations after the experiment in the vicinity of the transversal lines showed that at these

446 locations the grain size distribution of the soil was modified. The finer materials were removed
447 and were likely transported downstream while the larger particles were compacted and re-
448 organized to develop a thicker shield layer than in the rest of the flumes. These observations are
449 compatible with the hypothesis of higher rainfall rate and kinetic energy due the overlapping of
450 adjacent sprinklers.

451 Figure 10 near here

452 Fig. 10 shows the cumulative distributions of elevations for each of the flumes, before and
453 after the experiments. The curves confirmed an average change in elevation of about 2.5 cm for
454 each flume. Changes in soil elevation were roughly consistent among the different flumes,
455 although close inspection showed that the shape of each curve changed slightly. These small
456 changes indicated that the erosion was not uniform but some areas were locally more eroded.
457 The magnitude of the changes further confirmed that rills did not occur in these experiments.

458 The cumulative mass per unit width eroded from each flume is shown in Fig. 11. Each flume
459 showed a short initial transient followed by a nearly steady erosion rate. The initial transient
460 lasted until 25 min, consistent with the behavior observed in Figs. 6-9. Flumes 1 and 2 had a
461 comparable rate. Flume 4 showed a much reduced erosion rate throughout. Returning to flume 3,
462 it was observed that the erosion rate was very similar to that in flumes 1 and 2. It is possible that
463 the small but consistent reduction of total erosion in flume 3 was due to the impact of sediments
464 adhering to the barriers delineating each flume. The amount of material adhering to the barriers
465 is given in Table 1.

466 The elevation changes measured in the experiments are mainly due to a combination of two
467 processes, (i) erosion and (ii) soil compaction and consolidation from raindrop impact and

vibrations of the experimental apparatus. According to Fig. 11 the total amount of eroded sediment per unit area collected from flumes 1-3 was around 4.2 kg m^{-1}, while in flume 4 it was about 2.8 kg m^{-1}. In terms of mass per surface area, flumes 1-3 lost about 0.7 kg m^{-2} of the original soil, whereas flume 4 lost on average 0.47 kg m^{-2}. Using the initial measured bulk density, 1118 ± 20 kg m^{-3}, it is possible to estimate that the erosion event, on average, reduced the elevation of the original soil of about 0.6 mm. According to the DTM, the soil surface elevation decreased about 2.5 cm and therefore compaction/consolidation must have been responsible for the majority of this. Observations taken after the erosion event showed that the superficial soil layer (1-2 cm) was compacted and consolidated more than the rest of the profile. The dry bulk density of the top soil (up to a depth of 1-2 cm) was measured after compaction/consolidation, and a value of 1554 ± 96 kg m^{-3} was found. Twelve samples were used to compute this value, and it was observed that the spatial variability of the bulk density was relatively large, with values up to 1711 kg m^{-3}. Based on visual observations it was concluded that only the top soil layer compacted during the rainfall event and developed, after drying at least, a surface seal. It was also observed that the density of the upper 15-20 cm – the layer that was re-ploughed and that had a low bulk density before the experiment – increased, although the final bulk density was smaller than that of soil surface layer. It is expected that raindrop energy caused part of the observed compaction, but also there was likely soil settlement due to vibrations of the apparatus caused by mechanical action of the sprinklers.

The observations taken during and after the experiment, as well as the DTM data, highlight the impact of the collector's location on eroded soil. This collector location in flume 4 generated additional deposited sediment upstream from the collector. It is clear that, even though the initial surface elevation was uniform near the flume exit, the flume drainage point created a flow

nonuniformity similar to that in a soil column where flow contraction is present (e.g., Barry, 2009). Material detached by rainfall in this region is transported less relative to the fast-flowing region, with the effect that larger particles are preferentially deposited and finer particles removed. A sample of this deposited material was analyzed for the size fraction distribution. Consistent with the "flow-filtering" effect, about 80% of the deposited material (Fig. 2), which was collected from the opposite corner of collector's location of the flume 4, is composed of larger particles, i.e., finer particles were removed preferentially via suspension in the overland flow.

Figure 11 near here

3.2. Modeling

Given the consistent behavior of flumes 1-2 and flumes 3-4, the model was calibrated on flumes 1 and 3, and the optimized parameter sets were applied to flumes 2 and 4. Since the sediment class with grain diameters in the range 2-20 μm contained the largest proportion of the soil material (Table 2), the priority during the fitting was given to adjusting the model to reproduce the experimental data for this class. The allowed search range for each parameter was constrained – when possible – accounting for previous results and physical meaning of each parameter. In particular, according to the theory underlying the H-R model, the detachment rate of the original soil should always be smaller than that of the shield layer. With respect to the mass required to complete the shield, m_t^*, estimation of a reasonable parameter range is difficult, and therefore the search was not constrained, and conclusions on the likelihood of the parameter that best reproduced the experiments were drawn a posteriori. The thickness of the deposited layer of eroded material that covers the original soil, z, can be estimated from the mass per unit area, m_t^*:

$$m_t^* = (1-\eta)\rho_s z, \quad (7)$$

where ρ_s is the solid density of the sediments, η is the porosity of deposited layer and z is the depth of deposited layer. Application of Eq. (7) is difficult because the porosity of the deposited layer is unknown and variable in space. In the following, to compute the approximate thickness of the layer and compare with previous results, we assumed an average porosity of 0.35 and a solid density of 2500 kg m^{-3}.

In all the calibrations the overland flow depth, *D*, was fixed. During the erosion experiments it was found that the thickness of the overland water was variable in the range 5-10 mm. According to our preliminary numerical experiments, the best fit was achieved with a thicker layer of water, and consequently *D* was fixed to 9 mm.

The same numerical experiments were used to assess the sensitivity and correlation of the H-R model parameters. To this end, the Jacobian and covariance matrices were constructed (e.g., Hill and Østerby, 2002). It was found that the parameters were strongly correlated (> 0.99). This raised the question of the uniqueness of the estimated parameters, and indicated that parameter ranges should be constrained and when possible independently estimated. The uniqueness problem was confirmed by the confidence interval of the optimized parameters that was very large (and for this reason it is not reported in the following). The most influential parameter was the overland flow depth, *D*, followed by the mass required to complete the shield layer, m_t^*. According to Sander et al. (1996), when spatial effects are neglected, the steady state sediment concentration only depends indirectly on the overland flow depth through *a* and a_d. Correct identification of the average overland flow depth is therefore key to reproduce the short-time peak in the sediment breakthrough. The attachment/detachment coefficient, *a*, had a similar but much smaller sensitivity. This further indicates that it would be useful to identify possible

physical constraints for m_t^* because it is likely that otherwise the optimization process is mainly driven by this parameter.

The parameter sets that were found to provide the best fit are reported in Table 3, together with the approximate thickness of the shield layer computed using Eq. (7), and two metrics for the goodness-of-fit: RMSE and the correlation coefficients (r^2) between model and experimental data for class 2 (with the largest fraction of particles) in each flume. The adjusted velocities are given in Table 4. The set of parameters calibrated on one of the experiments discussed by Tromp-van Meerveld et al. (2008) is also reported in the bottom line of Table 3. The experiments of Tromp-van Meerveld et al. (2008) were conducted on the same flume used in this study. Details of their experimental setup are reported in Table 1. In particular it should be noted that in the experiments of Tromp-van Meerveld et al. (2008) the precipitation rate was lower than in our experiments, their flume was 2-m wide and their soil was more abundant in fine particles resulting in a smaller infiltration rate.

Table 3 near here

3.2.1. Flumes 1 and 2

Model predictions for flumes 1 and 2 are shown together with the experimental data in Figs. 6 and 7. With the optimized values for flume 1 and the measured settling velocities, the model reproduces well the total sediment concentration and the sediment breakthrough curves for the fine and mid-size granulometric classes of both flumes. After adjusting the settling velocities (Table 4), the comparison for the fine and mid-size classes was slightly improved (slightly higher r^2 and lower RMSE), and the model was also able to fit with reasonable accuracy the measured sediment concentrations for the larger particles, except the class with grains larger than 1 mm.

559 However, as already pointed out, for this class the experimental data were highly scattered and
560 did not show a clear trend. Interestingly, it was found that only the settling velocities of two
561 classes with mid- and coarse dimensions (100-315 μm and 315-1000 μm) had to be reduced to
562 improve the fitting. Tromp-van Meerveld et al. (2008) reported that the settling velocity of these
563 classes was difficult to determine and more scattered than for the finer and coarser particles. This
564 might indicate that, when the transverse (relative to flow direction) length scale is large enough
565 to avoid the effect of the boundaries and to get a good average flow behavior, for the fine and
566 mid-size particles the settling velocities estimated using Stokes' law or measured in the
567 laboratory are representative of the effective value observed at the larger scale. Instead, for the
568 coarser classes, modeling results indicate that there is a mechanism that reduces the effective
569 settling velocity. The experimental data did not allow further investigations of this aspect, but a
570 possible explanation is that the settling velocity does not well describe the motion of the heavier
571 particles, i.e., they do not move suspended in the water but via rolling or saltation (Asadi et al.,
572 2007; Hairsine and Sander, 2009; Heng et al., 2009).

573 In particular, the model reproduced both the long and short time behavior observed in the
574 data. In other words, this indicates that the model can represent well both the steady state
575 behavior, which is achieved when the shield layer fully develops and there is no further
576 detachment from the original soil, and the initial transient behavior, when two processes,
577 detachment from the original soil and from the shield layer contribute to suspend the soil
578 particles.

579 The H-R model with parameters optimized on flume 1 was able to reproduce the
580 measurements on flume 2, although less accurately. For the small soil particles, the model
581 slightly underpredicts the steady state behavior but captures satisfactorily the short-time peak and

582 subsequent decay observed in the sediment breakthrough curves, whereas for the mid- and
583 coarse-size classes the steady state is fully reproduced but the short time behavior is not. In
584 particular for the four larger size classes, in the initial 40 min the model simulations with
585 measured velocities slightly underestimated the measurements, whereas with the adjusted
586 velocities the data were overestimated. This further confirms the sensitivity of the settling
587 velocities to the length scale transverse to flow direction.

588 Optimized model parameters fit well within the ranges reported in the literature (e.g., Sander
589 et al., 1996, Gao et al., 2005). The three fittings (manual trial-and-error, automatic with measured
590 velocities and automatic with modified velocities) resulted in consistent estimates for the
591 detachability of both the original soil and of the shield layer. Moreover the detachability of the
592 shield layer is also consistent with the value reported by Tromp-van Meerveld et al. (2008). The
593 mass of soil required to complete the shield layer instead is significantly different, and varies
594 over two orders of magnitude. In terms of thickness of the shield layer z, the estimated value
595 varies from a maximum of 3 mm down to 0.03 mm when the settling velocities are adjusted. The
596 latter value is clearly non-physical since soil grains have a comparable size. The H-R model
597 assumes that a homogeneous shield layer develops over the entire eroded zone. In practice,
598 however, due to the irregular topography and composition of the soil it is likely that its thickness
599 was variable, with zones where the material was only removed and others where it accumulates.
600 The calibrated value is therefore an average over the entire surface, and reflected this spatial
601 variability. The effective size of the shield layer is however very difficult to measure in realistic
602 setups, and therefore comparison with model predictions cannot be made easily. Visual
603 observations however confirmed its spatial heterogeneity.

3.2.2. Flumes 3 and 4

Flumes 3 and 4 had a similar configuration and therefore it was anticipated that parameters optimized on flume 3 could be applied directly to flume 4. Overall, the model was able to reproduce the measurements of both flumes. For the fine particles, the fit was satisfactory ($r^2 >$ 0.98) and both the transient and long term behavior were reproduced. Instead, the concentrations at steady state of the larger classes (100-315, 315-1000 and > 1000 μm) were underestimated and subsequently the total sediment concentration was under-predicted. For the mid-size classes, the model reproduced the pattern found in the data, although the fitting was not completely satisfactory, even after adjusting the settling velocities. This is likely due to the important effect of the flume boundaries and asymmetries in the flow field. The model assumes uniform water flow and sediment concentrations. Close to the boundaries this is clearly not the case: Since the overland flow velocity was smaller, the mid-size and coarse particles were more easily deposited. In addition, a proportion of the mid-size grains ejected by raindrop splash remained physically attached to the wall (Fig. 2 reports the grain size distribution of the material attached to the walls).

The differences in model predictions between flumes 3 and 4 further confirmed the hypothesis concerning the effect of the outflow boundary condition. For these flumes, the largest difference between model and measurements was observed for the size classes (100-315, 315-1000 and > 1000 μm). It was discussed previously (§3.1.3) that the composition of the discharged sediments was affected strongly by the position of the drainage pipe. Its asymmetric position resulted in a non-uniform flow field that created a low-velocity zone near the downstream end of the flume, where coarse particles settled, as confirmed by the grain size distribution of the deposited material (Fig. 2).

The estimated detachabilities, a, were consistent with previous findings, and also the mass required to complete the shield layer, m_t^*, was similar (Sander et al., 1996). Concerning the shield layer, it is however not clear whether this is a realistic. The estimated thickness of the shield layer varies between about 1 and 5 mm, as calculated using Eq. (7). These values are comparable to previous estimates (Sander et al., 1996; Tromp-van Meerveld et al., 2008) and to measurements performed on very small setups (Heilig et al., 2001). Despite this, for flumes 3 and 4, with the optimized parameters the model predicts that the shield layer never fully develops over the course of the experiment, i.e., $m_t < m_t^*$. Its fractional thickness, H, always remained smaller than 0.5, which is different to the findings of Hairsine and Rose (1991a,b) and Sander et al. (1996). The optimization procedure also resulted in a larger value of m_t^* for our experiments as compared with that found in Sander et al. (1996). With a larger m_t^*, a greater total deposited mass m_t is required for the deposited layer to provide the same level of protection as that for a smaller m_t^*, and this takes longer to accumulate.

4. Discussion

The different behavior of H among flumes 1-2 and 3-4 could be explained as follows. For all flumes, the same soil was used and it was prepared in the same manner. The shield layer development follows a similar pattern in each pair of flumes 1-2 and 3-4 and so the results suggest that the size in the transverse direction is one of the keys to understand the shield layer formation. To be more specific, according to the model in flumes 1 and 2 the shield layer developed quickly and after a few minutes the steady state was reached. For flumes 3 and 4, instead, the shield layer never completely developed during the experiments. From the amount of sediment that adhered to the sides of the flumes during the experiment (Table 1), following Eq. (7) an estimate of the depth of "missing" sediment can be calculated as 0.030, 0.086, 0.25 and

650 0.23 mm, respectively, for flumes 1-4. The most physically reasonably values for m_t^* in Table 3
651 are those found by trial and error, which give the depth of the shield layer as 2.5 mm for flumes 1
652 and 2, and 1.2 mm for flumes 3 and 4. The amount of adhered sediment in flumes 1 and 2 would
653 not materially affect the deposited layer whereas for flumes 3 and 4, the "missing" amount is a
654 substantial proportion of the estimated m_t^*. For these two flumes a noticeable fraction of the
655 detached/suspended sediment belonging to the mid-size classes was trapped in or near the
656 barriers that divide the soil (Fig. 2). This material, which was transported to the sides of the
657 flumes in the initial stages of the experiment before overland flow depth was sufficient to
658 attenuate the raindrop erosion, would normally contribute to the formation of the shield (Tromp-
659 van Meerveld et al., 2008), but in these cases it was not available. Thus, the shield layer
660 formation in flumes 3 and 4 likely did not occur at the same rate as in flumes 1 and 2. Moreover,
661 part of each flume was partially protected in the transverse direction against the rainfall
662 detachment due to the shadowing effect of the walls. Both these mechanisms resulted in reduced
663 shield layer development such that the approach to a steady state shield layer occurred at a much
664 reduced rate in flumes 3 and 4.

665 The data collected from four flumes show that the measured sediment concentrations of the
666 finer particles are consistent. However, increasing particle size led to increasing variability in the
667 measured concentrations, perhaps in part because the concentrations of the larger particles were
668 sensitive to the specific flume conditions. A possible reason is that small particles, such as clay,
669 remained suspended in the overland flow, whereas the larger grains remained in contact with the
670 bed, especially in regions where the micro-topography is heterogeneous and water depth was
671 shallow (Asadi et al., 2007). That is, the bed's geometry created barriers and obstacles for the

672 water flow that were in turn sources and sinks of eroded sediments. This effect would be more
673 pronounced for larger particles.

674 The DTM revealed that after the erosion event the elevation of the flumes changed between 1
675 and 3 cm. These conditions could have affected locally the overland water depth and
676 consequently the hydraulics and the sediment transport mechanisms. DTM results suggested that
677 sediment transport alters between one- and two-dimensional mechanisms. In flume 1 (width of 1
678 m) and flume 2 (0.5 m), the topography changes were not homogenous in the transverse
679 direction, indicating that the second dimension could be important. In the narrower flumes, the
680 dominant soil erosion direction was parallel to water flow and erosion mainly occurred near the
681 center of the flumes. The non-uniform flow field induced near the exit of flume 4 significantly
682 modified the sediment breakthrough and, especially for the larger particles, limited model
683 applicability. It was found that the 1D model was able to reproduce most of the measurements
684 for the other flumes. This suggests that, so long as the length scale at which the 2D behavior is
685 important is much smaller than the transverse length scale, the model is able to reproduce the
686 average behavior of the soil undergoing erosion. On the contrary, it was observed that features in
687 the soil erosion flumes that significantly disturb the flow field and act as traps for the eroded
688 sediments hinder the ability of the model to reproduce the data in a consistent manner.

689 Based on the results of this study some recommendations can be drawn concerning sediment
690 sampling in case of flow asymmetries and/or limited transversal width. The spatial density of
691 sampling depends primarily on the goals of the experiment and the type of model that will be
692 applied (i.e., 0-, 1- or 2D). With 0- and 1D models it is appropriate to use an open area collection
693 point located at the downslope end of the plot (such as the collection point of flume 1), given that
694 the typical length scale of the flow disturbances is likely much smaller than the transverse width

of the sampled area. In this case the collected sediments represent the amount of sediment discharged and the collected data will be useful and representative for subsequent data analysis. If the flow field is instead irregular (i.e., the typical length scale for the asymmetries is comparable to the size of the plot) it would be probably more appropriate to use multiple collection points placed at different locations along the exit transect (not tested in the experiments reported here). In this situation the use of a 2D simulator would probably be beneficial (Nord and Esteves, 2005). In small scale field studies the flow field is often asymmetric, since the topography of the slopes is normally irregular and numerous obstacles are present (such as stones, vegetation, etc.).

The experiments and accompanying analyses showed that raindrop splash affects sediment breakthrough at the short time scale in situations where the raindrop energy is relatively high, as in these experiments. Additionally, the experiments started with a soil that had a low bulk density and was relatively dry. These conditions generated pronounced sediment concentrations for all the size classes immediately after the commencement of the overland flow. The high initial concentrations were however most apparent for the finer particles while for the mid-size and coarse soil particles the peak was attenuated, presumably due to soil surface irregularities and bed topography. Experimental results showed that the raindrop splash process led to high sediment concentrations at the beginning of the erosive event, defined as the time when overland flow first appeared at the end of the flume – this is a “first-flush” effect. In addition, all size classes contributed to the early sediment concentration peak.

To summarize, experimental results showed three types of behavior. First, raindrop splash dominated the response of the larger flumes (1 and 0.5 m). Second, the effect of raindrop splash was attenuated in the sediment concentration breakthroughs of the data collected from the

718 narrower flumes (0.25 m). Third, the boundary condition-induced asymmetry in flume 4 affected
719 markedly the concentrations of the mid-size and the larger particles.

720 We now consider the internal parameter consistency of the model (parameters given in Table
721 3). When the parameters (a, a_d and m_t^*) were adjusted manually ("trial and error", Table 3) and
722 used to predict the sediment concentrations of all flumes, the numerical approximations could
723 represent the total sediment concentrations well but the simulations of the individual size classes
724 were inadequate. However, when these parameters were estimated using a parameter estimation
725 procedure, according to each pair of flumes 1-2 and 3-4, the prediction of the individual size
726 classes was improved (Figs. 6-9). The best-fit values of a (detachability of the original soil)
727 changed significantly between each pair of flumes, with flumes 1 and 2 having a much greater
728 detachability. This is consistent with the foregoing discussion on the relative effect of the flume
729 barriers. With relatively more sediment adhering to the barriers in flumes 3 and 4, the soil
730 detachability decreased, presumably because the model does not account for sediment removal.
731 On the other hand, the values of a_d (detachability of the deposited soil) are fairly consistent. We
732 suggest that this is because this parameter is sensitive to the steady state (or long time) sediment
733 concentrations. It is thus unaffected by the initial transient phase when sediment is removed to
734 the barriers by rainfall splash. The optimized values of m_t^*, vary significantly. Considering the
735 largest difference (0.42 mg cm^{-2} and 80 mg cm^{-2} for each pair of flumes, 1-2 and 3-4), it is clear
736 that these values cannot be as physically reasonable since they lead to either very small (flumes 1
737 and 2) or very large (flumes 3 and 4) shield layer thicknesses. However, we have already pointed
738 out that the model parameters are highly correlated and so the best-fit values cannot be regarded
739 as unique. This situation would be improved if means to estimate parameters independently or to
740 constrain them using different types of data sets were employed. This finding supports that of

741 Barry et al. (2010) who, using a simplified version of the H-R model, showed that sediment
742 concentrations in the effluent could be explained by different assumptions applied to the H-R
743 model. They suggested that data on the deposited layer, if such data could be reliably obtained,
744 would help constrain the model applied.

745 **5. Summary and Conclusions**

746 A suite of laboratory experiments was conducted to analyze and understand flux and
747 composition of eroded sediments and to test the applicability of the 1D H-R model in the
748 presence of rainfall splash and irregular overland sheet flow. The flume was divided into four
749 plots with identical soil and surface preparation, but with different widths. The eroded sediments
750 were collected at the downstream end of the flume, and analyzed to characterize the total
751 discharged mass and the grain size distribution. These observations were complemented with
752 high-resolution laser scanning of the surface (used to generate a DTM of the soil), and direct
753 visual observations. It was found that a consistent short time peak was generated for all
754 individual size class concentrations, indicating that the splash effect was dominant in the wider
755 flumes (1 and 2). However, the peak partially disappeared in the data collected from the
756 narrower flume (3). For this flume only the finer particles showed a short-time peak. The mid-
757 size and larger particles were not discharged, but accumulated on and near the solid lateral
758 boundaries. This indicates that obstacles (i.e., stones, pebbles, vegetation) and topographic
759 sediment traps are likely to affect the composition of the removed sediment. The data collected
760 on flume 4, where the flow field was irregular and non-symmetric due to the off-set flow
761 collection point, further highlighted that irregular patterns of runoff affect sediment transport rate
762 and grain size distribution.

763 The H-R model was calibrated to the experimental results by adjusting the detachability of the
764 original soil, the detachability of the deposited layer and the mass per unit area needed to
765 complete the shield layer. After extensive investigations, it was concluded that the H-R model
766 represented well the total sediment concentrations as well as those of the fine and mid-size size
767 classes. However, the H-R model calibration could not provide physically significant parameters
768 when the transverse width of the flume experiment was below/around a threshold value related to
769 lateral splash length. Additionally, for all flumes, the model was not able to predict well the
770 breakthrough of the larger particles. For the coarse grains, the sediment transport mechanism
771 incorporated in the H-R model might be not fully appropriate. In that case, the identification of
772 reasonable settling velocities is difficult (Beuselinck et al., 2002; Asadi et al., 2007; Tromp-van
773 Meerveld et al. 2008), and likely to remain so in the analysis of future experiments.

774 Model fitting to the data yielded reasonably close predictions of the total sediment
775 concentrations, and of the different size classes. However, the parameter values themselves could
776 not be considered as highly reliable given the high correlation between them. Means to constrain
777 independently parameters would thus be valuable. In summary, the experimental data and
778 accompanying analyses showed that (i) raindrop splash can have a dominant effect on short-time
779 erosion behavior in situations where the rainfall drop energy is relatively high; (ii) the H-R
780 model does not include sufficient mechanistic detail to account for high-energy raindrops that
781 move sediments considerable distances; (iii) for laboratory flumes with uniform soil conditions,
782 there is a minimum transverse length scale over which the H-R model (or any other erosion
783 model) is likely applicable, and that one factor influencing this minimum scale is the
784 characteristic splash length scale; (iv) for narrow flumes the amount of sediment adhering to the
785 lateral flume boundaries affects the evolution of the erosion process; and (v) that boundary

condition-induced asymmetry markedly reduces the applicability of the 1D H-R (and likely other) erosion model.

Acknowledgments

This work was supported by the Swiss Natural Science Foundation (grant 200021-113815).

References

Asadi, H., Ghadiri, H., Rose, C.W. and H. Rouhipour, H., 2007. Interrill soil erosion processes and their interaction on low slopes. Earth Surface Processes and Landforms, 32(5): 711-724.

Baril, P., 1991. Erodibilité des sols et érodabilité des terres: Application au plateau vaudois. Ph.D. Thesis, Ecole Polytechnique Fédérale de Lausanne (EPFL), Lausanne, Switzerland, 218 pp.

Bajracharya, K. and Barry, D.A., 1995. MCMFIT: Efficient optimal fitting of a generalised nonlinear advection-dispersion model to experimental data. Computers and Geosciences, 21(1): 61-76.

Barry, D.A., 2009. Effect of nonuniform boundary conditions on steady flow in saturated homogeneous cylindrical soil columns. Advances in Water Resources, 32(4): 522-531.

Barry, D.A., Sander, G.C., Jomaa, S., Heng, B.C.P., Parlange, J.-Y., Lisle, I.G. and Hogarth, W.L. 2010. Exact solutions of the Hairsine-Rose precipitation-driven erosion model for a uniform grain size soil. Journal of Hydrology, 389(3-4): 399-405.

Bertuzzi, P., Rauws, G. and Courault, D., 1990. Testing roughness indexes to estimate soil surface-roughness changes due to simulated rainfall. Soil and Tillage Research, 17(1-2): 87-99.

808 Beuselinck, L., Govers, G., Steegen, A. and Quine, T.A. 1999. Sediment transport by overland
809 flow over an area of net deposition, Hydrological Processes, 13(17): 2769-2782.
810 Beuselinck, L., Hairsine, P., Sander G.C. and Govers, G., 2002. Evaluating a multiclass net
811 deposition equation in overland flow conditions. Water Resources Research, 38(7): doi:
812 10.1029/2001WR0000250.

813 Christiansen, J.E., 1942. Irrigation by sprinkling, California Agricultural Experimental Station,
814 University of California, Berkeley, USA.
815 Cogo, N.P., Moldenhauer, W.C. and Foster, G.R., 1983. Effect of crop residue, tillage-induced
816 roughness, and runoff velocity on size distribution of eroded soil aggregates. Soil Science
817 Society of America Journal, 47(5): 1005-1008.
818 Darboux, F. and Huang, C., 2003. An instantaneous-profile laser scanner to measure soil surface
819 microtopography. Soil Science Society of America Journal, 67(1): 92-99.
820 Darboux, F. and Huang, C.H., 2005. Does soil surface roughness increase or decrease water and
821 particle transfers? Soil Science Society of America Journal, 69(3): 748-756.
822 Gao, B., Walter, M.T., Steenhuis, T.S., Parlange, J.-Y., Nakano, K., Rose, C.W. and Hogarth,
823 W.L., 2003. Investigating ponding depth and soil detachability for a mechanistic erosion
824 model using a simple experiment. Journal of Hydrology, 277(1-2): 116-124.
825 Gao, B., Walter, M.T., Steenhuis, T.S., Parlange, J.-Y., Richards, B.K., Hogarth, W.L. and Rose.
826 C .W., 2005. Investigating raindrop effects on transport of sediment and non-sorbed
827 chemicals from soil to surface runoff. Journal of Hydrology 308(1-4): 313–320.
828 Gomez, J.A., Darboux, F. and Nearing, M.A., 2003. Development and evolution of rill networks
829 under simulated rainfall. Water Resources Research, 39(6), 1148, doi:
830 10.1029/2002WR001437.

831 Gomez, J.A. and Nearing, M.A., 2005. Runoff and sediment losses from rough and smooth soil
832 surfaces in a laboratory experiment. Catena, 59(3): 253-266.
833 Hairsine, P.B. and Rose, C.W., 1991. Rainfall detachment and deposition-sediment transport in
834 the absence of flow-driven processes. Soil Science Society of America Journal, 55(2):
835 320-324.
836 Hairsine, P.B. and Rose, C.W., 1992. Modeling water erosion due to overland-flow using
837 physical principles. 1. Sheet flow. Water Resources Research, 28(1): doi:
838 10.1029/91WR02380.
839 Hairsine, P.B. and Rose, C.W., 1992. Modeling water erosion due to overland-flow using
840 physical principles. 2. Rill flow. Water Resources Research, 28(1): doi:
841 10.1029/91WR02381.
842 Hairsine, P.B., and Sander, G.C., 2009. Comment on "A transport-distance based approach to
843 scaling erosion rates: Parts 1, 2 and 3" by Wainwright, et al. 2008. Earth Surface
844 Processes and Landforms, 34(6): 882-885.
845 Hancock, G.R., Crawter, D., Fityus, S.G., Chandler, J. and Wells, T., 2008. The measurement
846 and modelling of rill erosion at angle of repose slopes in mine spoil. Earth Surface
847 Processes and Landforms, 33(7): 1006-1020.
848 Heilig, A., DeBruyn, D., Walter, M.T., Rose, C.W., Parlange, J.-Y., Steenhuis, T.S., Sander,
849 G.C., Hairsine, P.B., Hogarth, W.L. and Walker, L.P., 2001. Testing a mechanistic soil
850 erosion model with a simple experiment. Journal of Hydrology, 244(1-2): 9-16.
851 Heng, B.C.P., Sander, G.C. and Scott, C.F., 2009. Modeling overland flow and soil erosion on
852 nonuniform hillslopes: A finite volume scheme. Water Resources Research, 45, W05423,
853 doi: 10.1029/2008WR007502.

Hill, M.C. and Østerby, O., 2002. Determining extreme parameter correlation in ground water models. Ground Water, 41(4): 420-430.

Johnson, C.B., Mannering, J.V. and Moldenhauer, W.C., 1979. Influence of surface-roughness and clod size stability on soil and water losses. Soil Science Society of America Journal, 43(4): 772-777.

Le Bissonnais, Y., Cerdan, O., Lecomte, V., Benkhadra, H., Souchere, V. and Martin, P., 2005. Variability of soil surface characteristics influencing runoff and interrill erosion. Catena, 62(2-3): 111-124.

Legout, C., Leguedois, S. and Le Bissonnais, Y., 2005. Aggregate breakdown dynamics under rainfall compared with aggregate stability measurements. European Journal of Soil Science, 56(2): 225-237.

Legout, C., Leguedois, S., Le Bissonnais, Y. and Issa, O.M., 2005. Splash distance and size distributions for various soils. Geoderma, 124(3-4): 279-292.

Leguedois, S. and Le Bissonnais, Y., 2004. Size fractions resulting from an aggregate stability test, interrill detachment and transport. Earth Surface Processes and Landforms, 29(9): 1117-1129.

Leguedois, S., Planchon, O., Legout, C. and Le Bissonnais, Y., 2005. Splash projection distance for aggregated soils: Theory and experiment. Soil Science Society of America Journal, 69(1): 30-37.

Lisle, I.G., Rose, C.W., Hogarth, W.L., Hairsine, P.B., Sander G.C. and Parlange, J.-Y., 1998. Stochastic sediment transport in soil erosion, Journal of Hydrology 204(1-4): 217-230.

Mouzai, L. and Bouhadef, M., 2003. Water drop erosivity: Effects on soil splash, Journal of Hydraulic Research, 41(1): 61-68.

877 Nord, G., and Esteves, M., 2005. PSEM_2D: A physically based model of erosion processes at
878 the plot scale. Water Resources Research, 41, W08407, doi: 10.1029/2004WR003690.
879 Onstad, C.A., Wolfe, M.L., Larson, C.L. and Slack, D.C., 1984. Tilled soil subsidence during
880 repeated wetting. Transactions of the ASAE, 27(3): 733-736.
881 Parlange, J.-Y., Hogarth, W.L., Rose, C.W., Sander, G.C., Hairsine, P. and Lisle, I., 1999.
882 Addendum to unsteady soil erosion model. Journal of Hydrology, 217(1-2): 149-156.
883 Planchon, O., Esteves, M., Silvera, N. and Lapetite, J.M., 2000. Raindrop erosion of tillage
884 induced microrelief: Possible use of the diffusion equation. Soil and Tillage Research,
885 56(3-4): 131-144.
886 Proffitt, A.P.B., Rose, C.W. and Hairsine, P.B., 1991. Rainfall detachment and deposition-
887 experiments with low slopes and significant water depths. Soil Science Society of
888 America Journal, 55(2): 325-332.
889 Rieke-Zapp, D.H. and Nearing, M.A., 2005. Digital close range photogrammetry for
890 measurement of soil erosion. Photogrammetric Record, 20(109): 69-87.
891 Rudolph, A. Helming, K. and Diesel, H., 1997. Effect of antecedent soil water content and
892 rainfall regime on microrelief changes. Soil Technology, 10(1): 69-81.
893 Römkens, M.J.M., Heling, K. and Prasad, S.N., 2002. Soil erosion under different rainfall
894 intensities, surface roughness, and soil water regimes, Catena, 46 (2-3):103-123.
895 Rose, C.W., Williams, J.R., Sander, G.C. and Barry, D.A., 1983. A mathematical-model of soil-
896 erosion and deposition processes. 1. Theory for a plane land element. Soil Science
897 Society of America Journal, 47(5): 991-995.

898 Rose, C.W., Williams, J.R., Sander, G.C. and Barry, D.A., 1983. A mathematical-model of soil-
899 erosion and deposition processes. 2. Application to data from an arid-zone catchment.
900 Soil Science Society of America Journal, 47(5): 996-1000.
901 Rose, C.W., Yu, B., Ghadiri, H., Asadi, H., Parlange, J.-Y., Hogarth, W.L. and Hussein, J., 2007.
902 Dynamic erosion of soil in steady sheet flow. Journal of Hydrology, 333(2-4): 449-458.
903 Salles, C. and Poesen, J., 2000. Rain properties controlling soil splash detachment. Hydrological
904 Processes, 14(2): 271-282.
905 Sander, G.C., Hairsine, P.B., Rose, C.W., Cassidy, D., Parlange, J.-Y., Hogarth, W.L. and Lisle,
906 I.G., 1996. Unsteady soil erosion model, analytical solutions and comparison with
907 experimental results. Journal of Hydrology, 178(1-4): 351-367.
908 Sander, G.C., Parlange, J.-Y., Barry, D.A., Parlange, M.B. and Hogarth, W.L., 2007. Limitation
909 of the transport capacity approach in sediment transport modeling. Water Resources
910 Research, 43, W02403, doi: 10.1029/2006WR005177.
911 Stokes, G.G., 1851. On the effect of the internal friction on the motion of pendulums. Cambridge
912 Philosophical Society, IX(2): 8-106.
913 Tromp-van Meerveld, H.J., Parlange, J.-Y., Barry, D.A., Tromp, M.F., Sander, G.C., Walter,
914 M.T. and Parlange, M.B., 2008. Influence of sediment settling velocity on mechanistic
915 soil erosion modeling. Water Resources Research, 44, W06401, doi:
916 10.1029/2007WR006361.
917 van Dijk, A., Meesters, A. and Bruijnzeel, L.A., 2002. Exponential distribution theory and the
918 interpretation of splash detachment and transport experiments. Soil Science Society of
919 America Journal, 66(5): 1466-1474.

Viani, J.-P., 1986. Contribution à l'étude expérimentale de l'érosion hydrique. Ph.D. Thesis, Ecole Polytechnique Fédérale de Lausanne (EPFL), Lausanne, Switzerland, 239 pp.

Walker, J.D., Walter, M.T., Parlange, J.-Y., Rose, C.W., Tromp-van Meerveld, H.J., Gao, B. and Cohen., A.M., 2007. Reduced raindrop-impact driven soil erosion by infiltration. Journal of Hydrology, 342(3-4): 331-335.

925 **Table 1**

926 Summary of the conditions for the experiments in the four erosion flumes. The collector locations
927 are shown in Fig. 3. The conditions of one of the experiments conducted by Tromp-van Meerveld
928 et al. (2008) are also reported. Note that despite the different precipitation rate, the amount of
929 overland flow in H3 is comparable to that of experiments 1-4 because of the smaller infiltration
930 rate.

Flume	Collector	Width (m)	Duration (min)	Slope (%)	*P* (mm h^{-1})	Number of samples	Mass adhered (g)
1	1	1	160	2.2	60	42	301
2	2.1	0.5	160	2.2	60	40	419
2	2.2	0.5	160	2.2	60	29	
3	3	0.25	160	2.2	60	39	603
4	4	0.25	160	2.2	60	36	564
H3*	-	2	130	2.2	47.5	21	-

931 * Data from Tromp-van Meerveld et al. (2008)

Table 2

Overview of the seven particle size diameter classes with the corresponding measured settling velocities from Tromp-van Meerveld et al. (2008).

Size Class	Diameter (µm)		Proportion p_i	Settling velocity (m s^{-1})	
	From	To	(%)	From	To
1	0	2	4.6	8.0×10^{-8}	4.0×10^{-6}
2	2	20	26.6	4.0×10^{-6}	4.0×10^{-4}
3	20	50	13.3	4.0×10^{-4}	2.5×10^{-3}
4	50	100	5.6	2.5×10^{-3}	1.4×10^{-2}
5	100	315	13.6	1.4×10^{-2}	3.7×10^{-2}
6	315	1000	14.5	3.7×10^{-2}	6.9×10^{-2}
7	> 1000		21.8	6.9×10^{-2}	1.4×10^{-1}

Table 3

Optimized parameter sets obtained by fitting the experimental data for flume 1 and 3. For all simulations, the depth of the overland flow, D, was constant and equal to 9×10^{-3} m. The H-R model parameters for one of the experiments (carried out using the same flume) reported in Tromp-van Meerveld et al. (2008) are shown for comparison.

	Method	a (mg cm^{-3})	a_d (mg cm^{-3})	m_t^* (mg cm^{-2})	z (m)	r^2	*RMSE*
Flumes 1, 2	Trial and error	40	8800	40	2.5×10^{-3}	0.953	3.860
	Measured V_i	27	9320	9.0	0.55×10^{-3}	0.899	1.863
	Modified V_i	94	5246	0.4	0.02×10^{-3}	0.931	1.821
Flumes 3, 4	Trial and error	50	8700	20	1.2×10^{-3}	0.923	27.584
	Measured V_i	9.3	8308	75	4.6×10^{-3}	0.984	2.312
	Modified V_i	9.1	13842	80	4.9×10^{-3}	0.985	2.623
H3*	Trial and error	21700	6510	16	0.99×10^{-3}	NA	NA

* Data taken from Tromp-van Meerveld et al. (2008). Correlation coefficient and RMSE not available (NA).

941 **Table 4**

942 Settling velocities used to model the experimental data. The measured velocities are average values of the ranges reported in Tromp-
943 van Meerveld et al. (2008). Shaded in gray are velocities that were modified to improve the fitting. For flumes 1 and 2 the settling
944 velocity of two classes was decreased, whereas for flumes 3 and 4 the settling velocity of most classes was increased.

	Size class (µm)	< 2	2 – 20	20 - 50	50 - 100	100 - 315	315 - 1000	> 1000
All flumes	Measured V_i (m s^{-1})	5×10^{-7}	1.5×10^{-5}	7×10^{-4}	4×10^{-3}	2×10^{-2}	4×10^{-2}	6×10^{-2}
Flumes 1, 2	Modified V_i (m s^{-1})	5×10^{-7}	1.5×10^{-5}	7×10^{-4}	4×10^{-3}	4×10^{-3}	4×10^{-3}	6×10^{-2}
Flumes 3, 4	Modified V_i (m s^{-1})	3.7×10^{-6}	1.1×10^{-4}	2.5×10^{-3}	2.2×10^{-3}	5.3×10^{-2}	4.2×10^{-2}	1.0×10^{-1}

Figure Captions

1. Erosion flume
2. Flume dividers
3. Flow collection troughs
    a. Flume 1
    b. Flume 2
    c. Flume 3
    d. Flume 4
    e. Subsurface flow
4. Lake water supply
5. Water outlet tube
6. Collection troughs
7. To storm water drain
8. Rotating bar
9. Oscillator
10. Direction of oscillation
11. Compressor
12. Magnetic vane
13. Regulator
14. Manometer
15. Maximum oscillation amplitude ($\alpha = 90°$)
16. Actual water outlet ($\beta = 30°$)
17. Water jet

Note, the above material is to be included in Fig. 1, and placed below the accompanying figure

Fig. 1. Schematic overview of the EPFL erosion flume (modified from Tromp-van Meerveld et al., 2008). Note that the drainage system (item 3) was modified for the present experiments and that the flume was divided in 4 sections using the flume dividers (item 2).

Fig. 2. Grain size distribution of the original soil (solid line, squares), of the material deposited after the erosion experiment from the bottom corner of flume 4 (dashed line, circles) and of the materials removed from solid walls (gray line, diamonds). The material deposited on the solid walls is richer that the original soil in grains belonging to the mid-size classes, while that deposited in the left-bottom corner is depleted in the finer classes.

Fig. 3. Layout of the soil erosion device showing the four flumes. The location of the water/sediment collection points is shown at the bottom of the figure for each flume. Flumes 1 and 3 had a single, central collection point, flume 2 had two symmetrically located collection points (denoted 3b.1 and 3b.2) and flume 4 had a single, offset collection point. The sediment concentrations of flume 2 reported in the text are the average values of the concentrations measured in the water collected from points 3b.1 and 3b.2.

Fig. 4. DTM's of the flumes before and after the experiment. These images were generated after processing the data acquired using a high resolution laser scanner. The longitudinal lines within the images are the vertical (to a height of 10 cm above the initial soil surface) barriers that define the individual flumes. The excess of deposited sediment near the left bottom corner of flume 4 after the experiment was due to the non-uniform flow field induced by the offset location of the water (and sediment) collector. The grain size distribution of this material is shown in Fig. 2.

Fig. 5. Schematic diagram from Rose et al. (2007) illustrating the deposited layer z (t). When the shield layer fully develops, $z = z$ (m_t^*), the original soil is protected against erosion by raindrops. The dashes show the overall depth to which the soil is eroded (and replaced by deposited sediment).

Fig. 6. Measured sediment breakthrough curves and simulated results for flume 1. Model parameters were optimized on this dataset. The top left panel shows the total sediment concentration as well as the fractional coverage H. For this flume the shield layer develops quickly and reaches a value of about 96% within the first 10 min.

Fig. 7. Measured sediment breakthrough curves and simulated results for flume 2. The experimental data show a consistent maximum in the first 25 min, due to the effect of raindrop splash. The model parameters optimized on flume 1 were also used here. The model reproduces well most of the datasets.

Fig. 8. Measured sediment breakthrough curves and simulated results for flume 3. Model parameters were optimized on this dataset. The fine size classes are reproduced extremely well ($r^2 > 0.98$). According to the model, however, the shield layer never fully develops.

Fig. 9. Measured sediment breakthrough curves and simulated results for flume 4. The asymmetric location of the sediment collector affects mainly the coarse particles. Model parameters were not estimated, rather the optimized values for flume 3 were used.

Fig. 10. Cumulative distribution of the surface elevation before (top panel) and after (bottom panel) the erosion experiment. The four lines in each panel show the elevation distribution for each flume. From the analysis of the data it was found that, on average, the soil surface was reduced by about 2.5 cm during the soil erosion.

Fig. 11. Flux-averaged cumulative mass eroded from the soil per unit width as a function of time for the four flumes. Despite the different widths, flumes 1-3 exhibit a consistent behavior, while the amount of sediments discharged from flume 4 is significantly smaller, due to the asymmetric positioning of the sediment collector.

Figure 1

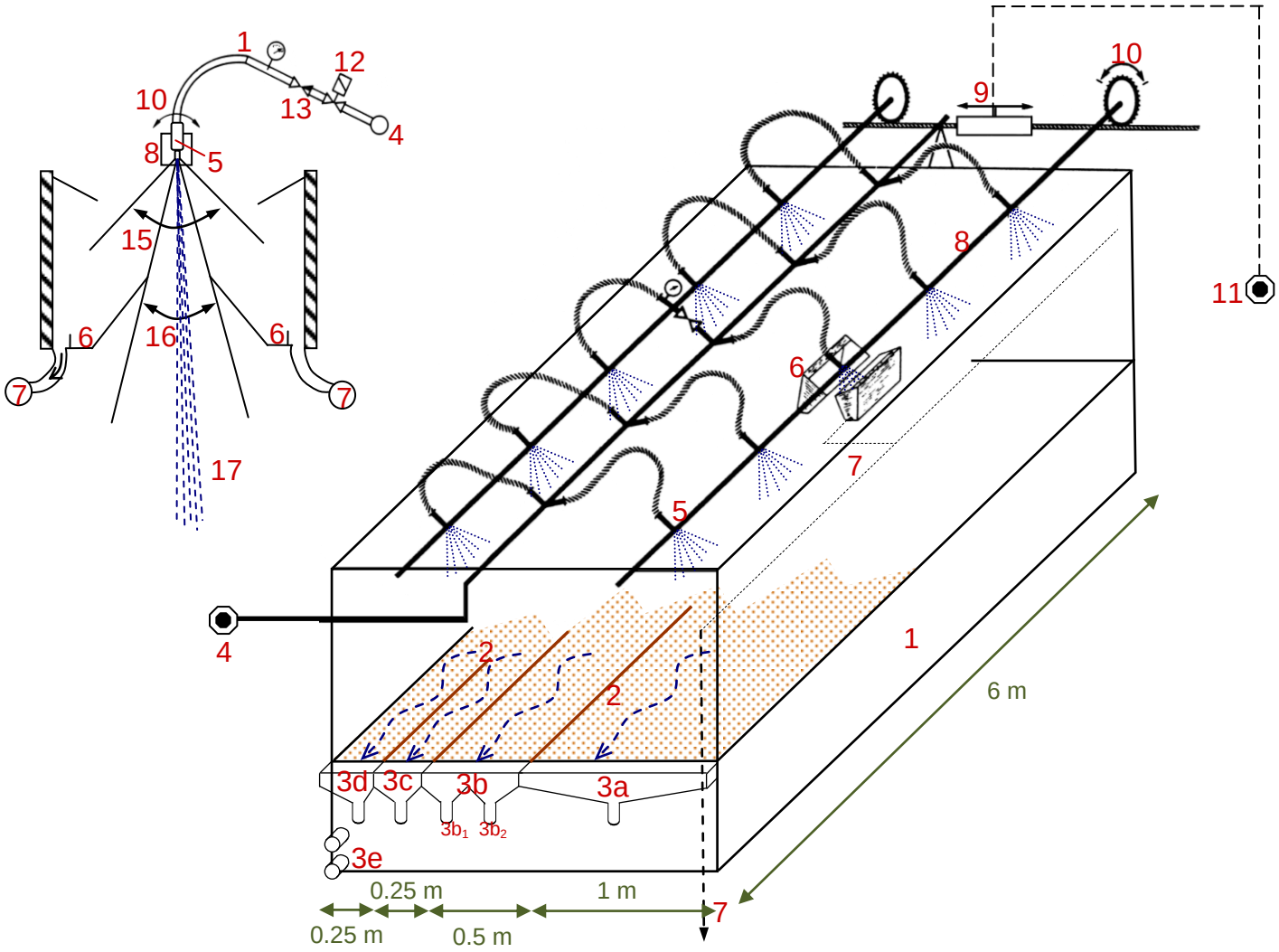
1
12
10
13
4
8
5
15
6
16
6
7
7
17
10
9
8
11
6
7
5
4
2
2
1
6 m
3d
3c
3b
3a
3b1
3b2
3e
0.25 m
1 m
7
0.25 m
0.5 m

Figure 2

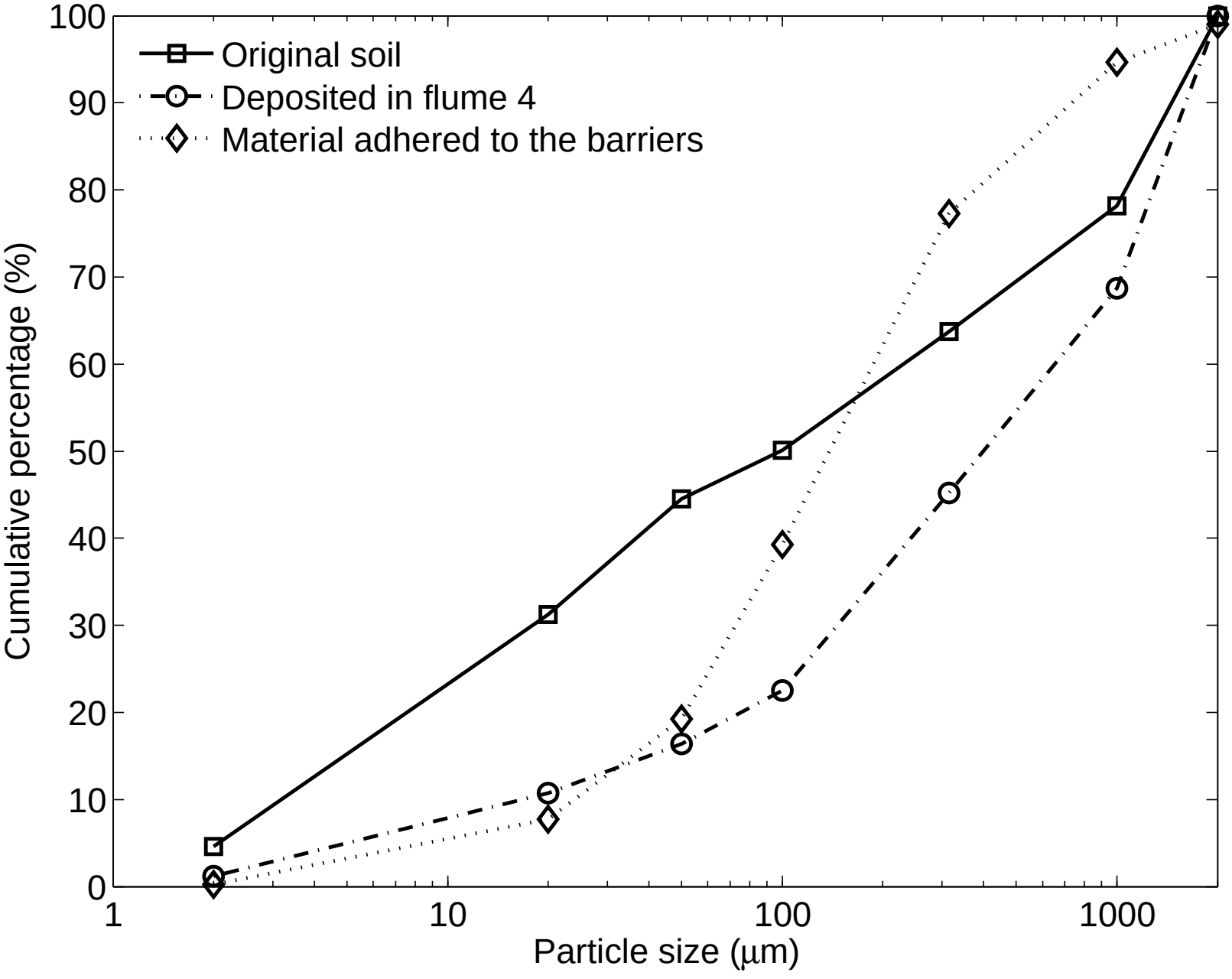
Original soil
Deposited in flume 4
Material adhered to the barriers
Cumulative percentage (%)
Particle size (μm)
0
10
20
30
40
50
60
70
80
90
100
1
10
100
1000

Figure 3

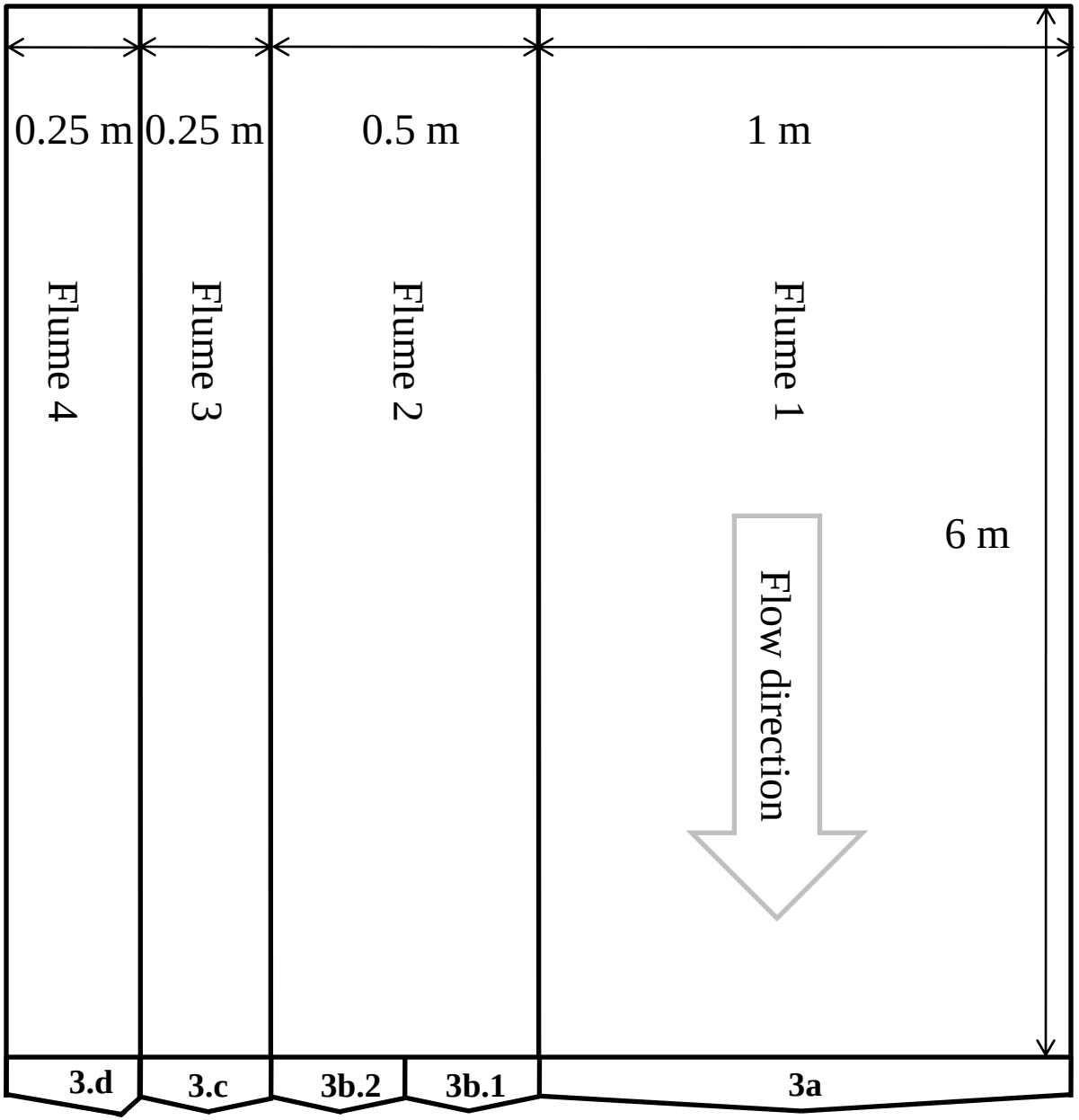
0.25 m
0.25 m
0.5 m
1 m
Flume 4
Flume 3
Flume 2
Flume 1
6 m
Flow direction
3.d
3.c
3b.2
3b.1
3a

Figure 4

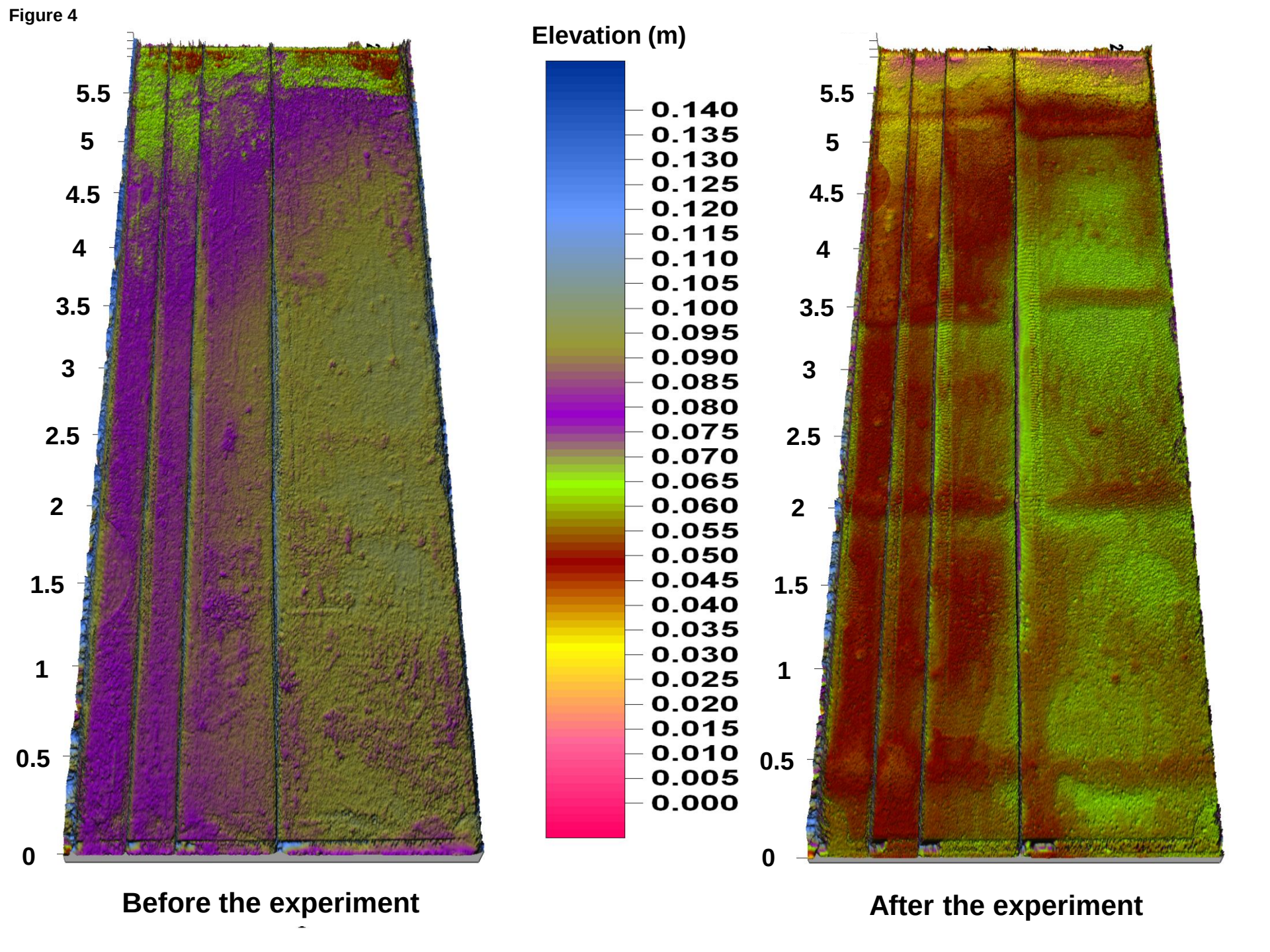
Elevation (m)
0.140
0.135
0.130
0.125
0.120
0.115
0.110
0.105
0.100
0.095
0.090
0.085
0.080
0.075
0.070
0.065
0.060
0.055
0.050
0.045
0.040
0.035
0.030
0.025
0.020
0.015
0.010
0.005
0.000
5.5
5
4.5
4
3.5
3
2.5
2
1.5
1
0.5
0
Before the experiment
After the experiment

Figure 5

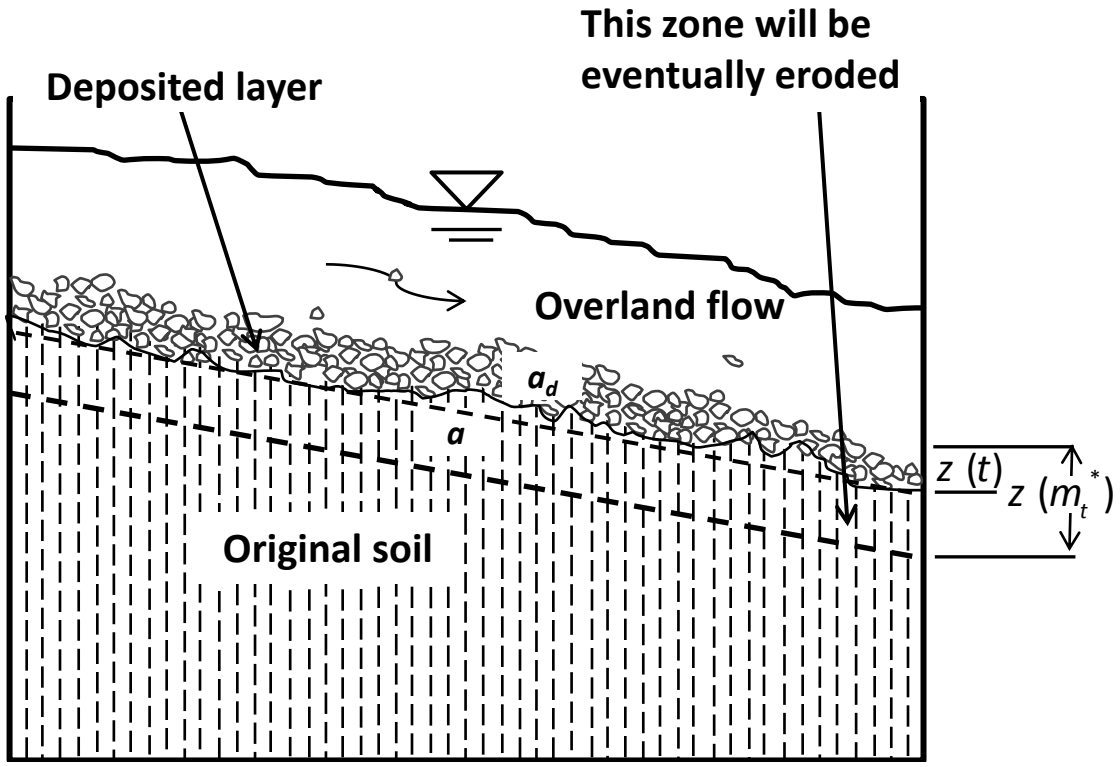
This zone will be
eventually eroded
Deposited layer
Overland flow
a_d
a
Original soil
$z\ (t)$
$z\ (m_t^*)$

Figure 6

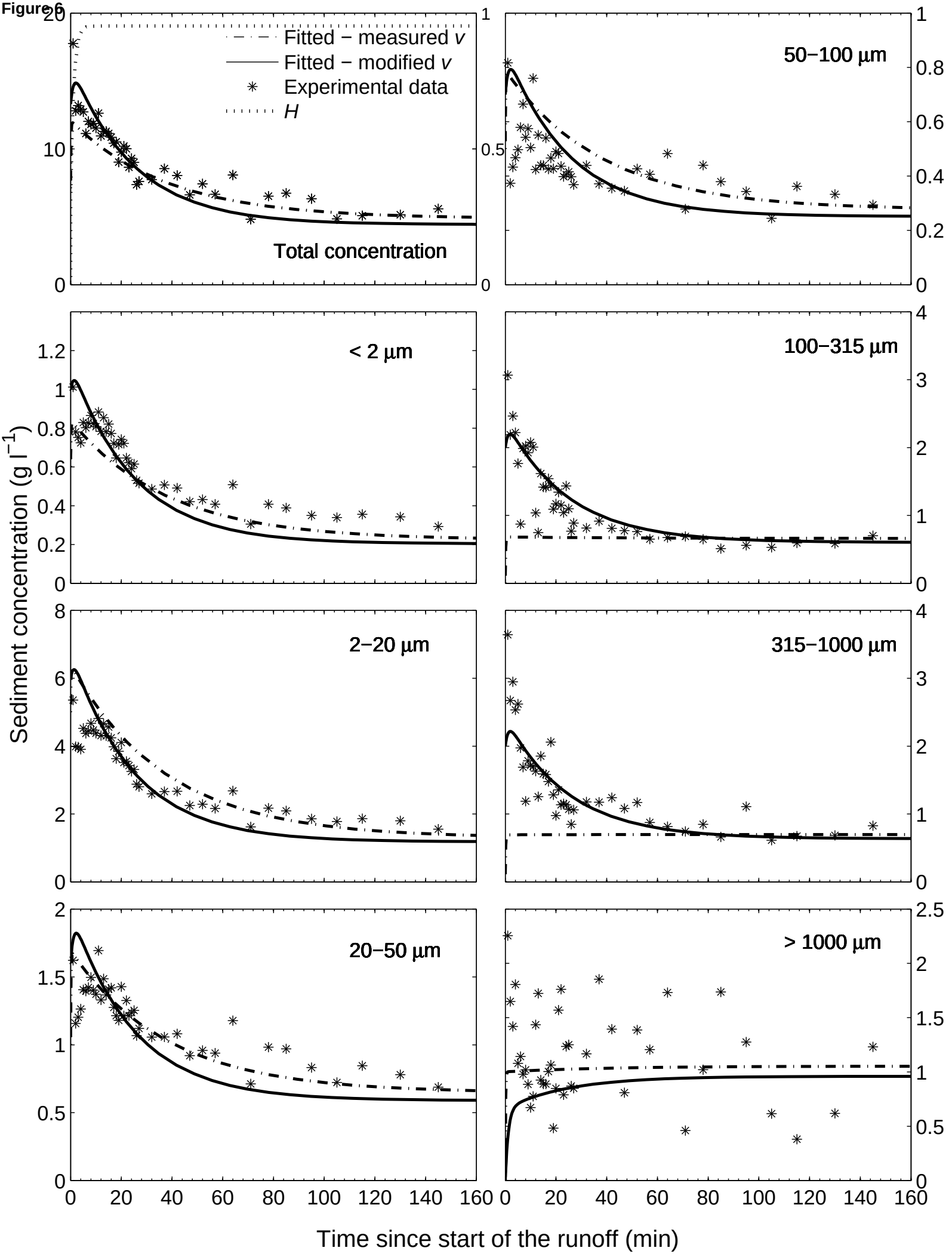
Fitted − measured v
Fitted − modified v
Experimental data
H
Total concentration
50−100 µm
< 2 µm
100−315 µm
2−20 µm
315−1000 µm
20−50 µm
> 1000 µm
Sediment concentration (g l−1)
Time since start of the runoff (min)

Figure 7

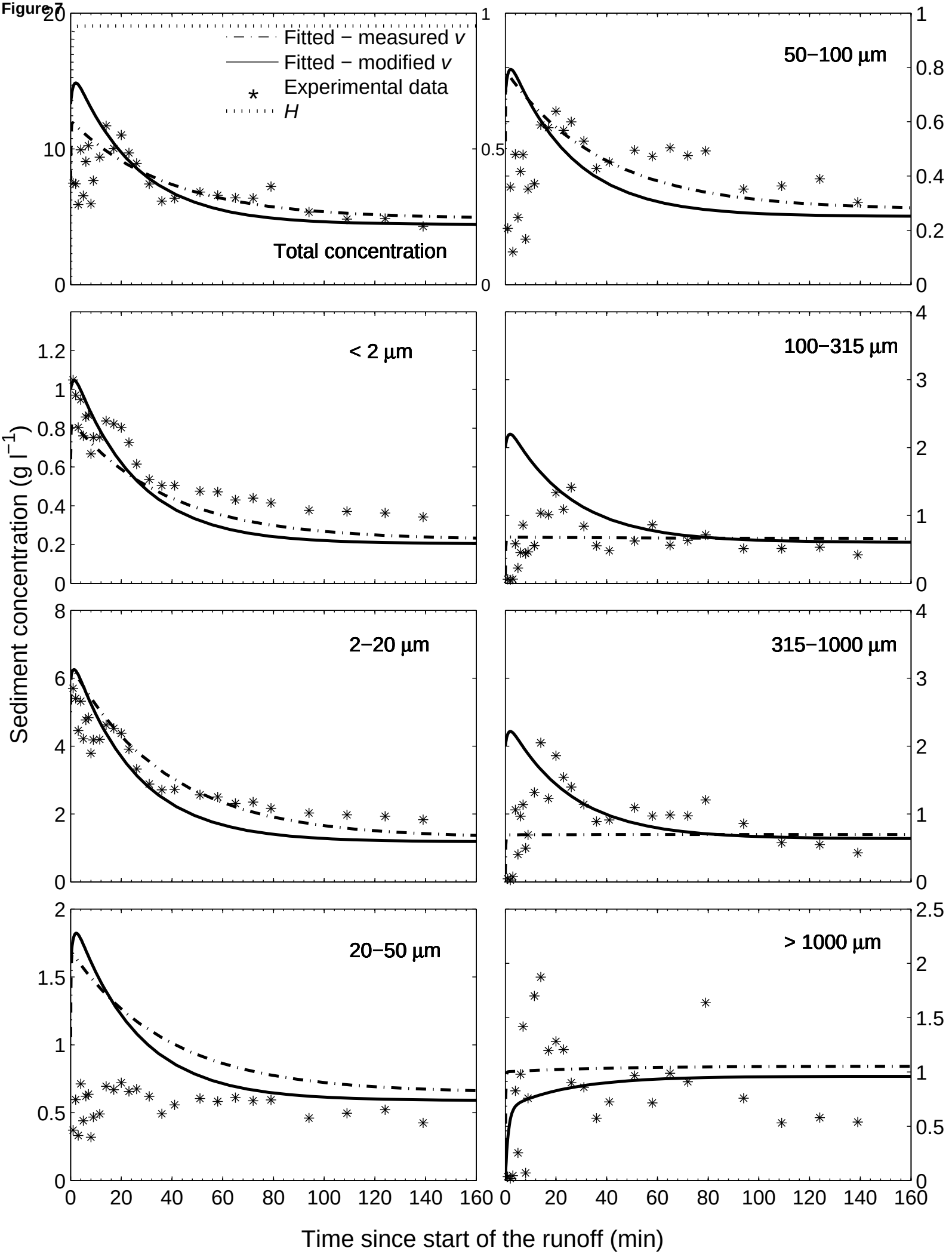
Fitted − measured v
Fitted − modified v
Experimental data
H
Total concentration
50−100 µm
< 2 µm
100−315 µm
2−20 µm
315−1000 µm
20−50 µm
> 1000 µm
Sediment concentration (g l−1)
Time since start of the runoff (min)

Figure 8

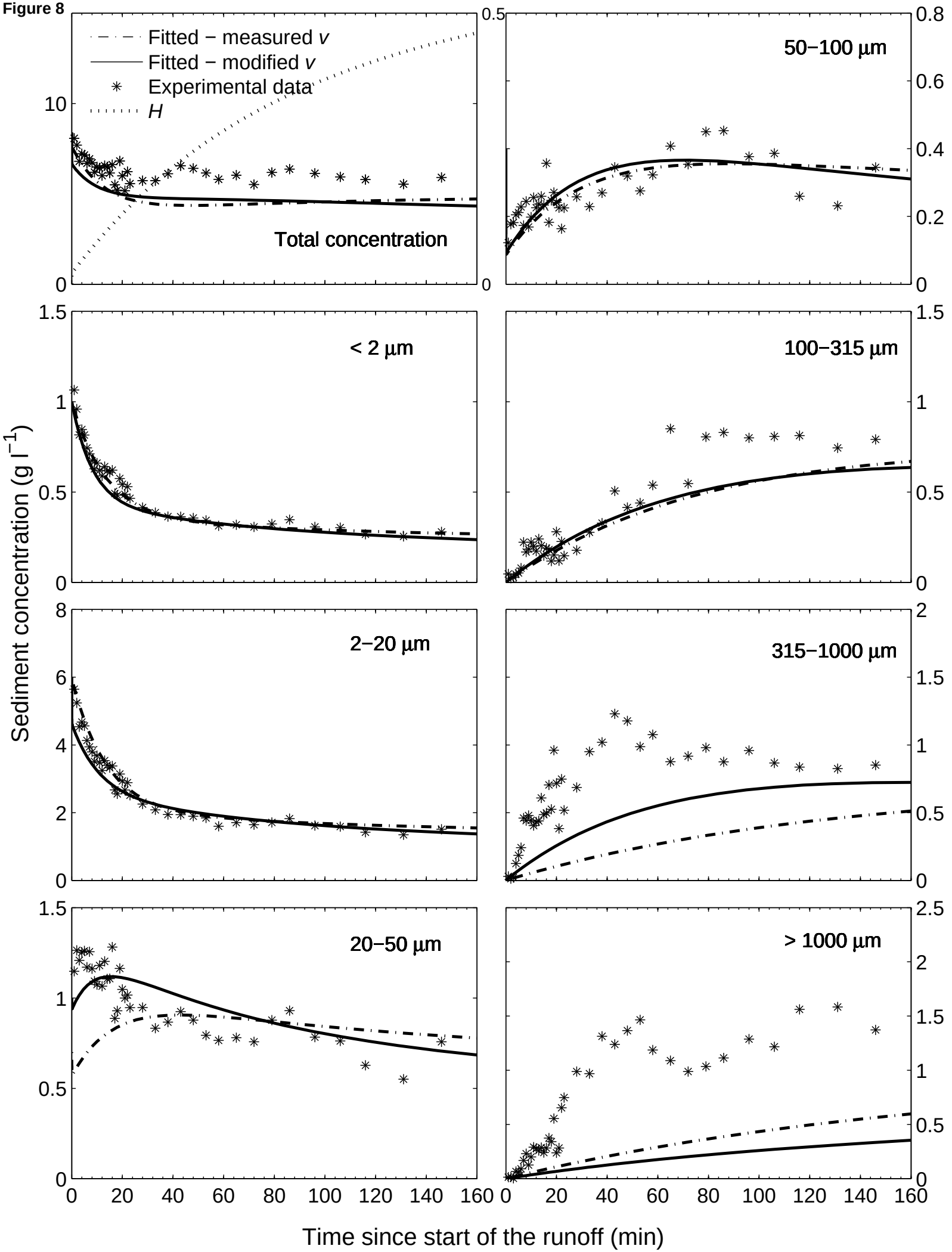
Fitted − measured v
Fitted − modified v
Experimental data
H
Total concentration
50−100 µm
< 2 µm
100−315 µm
2−20 µm
315−1000 µm
20−50 µm
> 1000 µm
Sediment concentration (g l−1)
Time since start of the runoff (min)

Figure 9

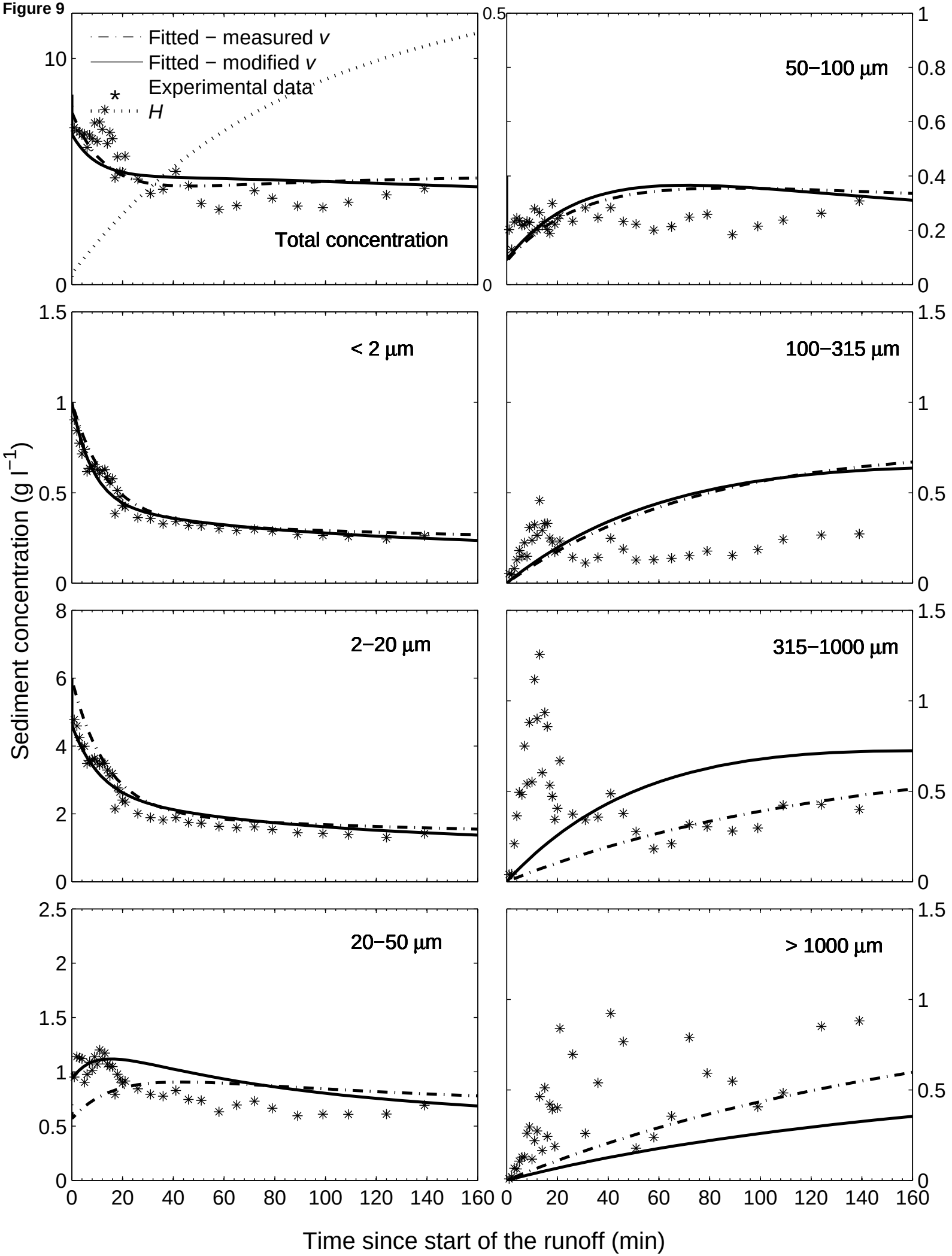
Fitted − measured v
Fitted − modified v
Experimental data
H
Total concentration
50−100 µm
< 2 µm
100−315 µm
2−20 µm
315−1000 µm
20−50 µm
> 1000 µm
Sediment concentration (g l−1)
Time since start of the runoff (min)

Figure 10

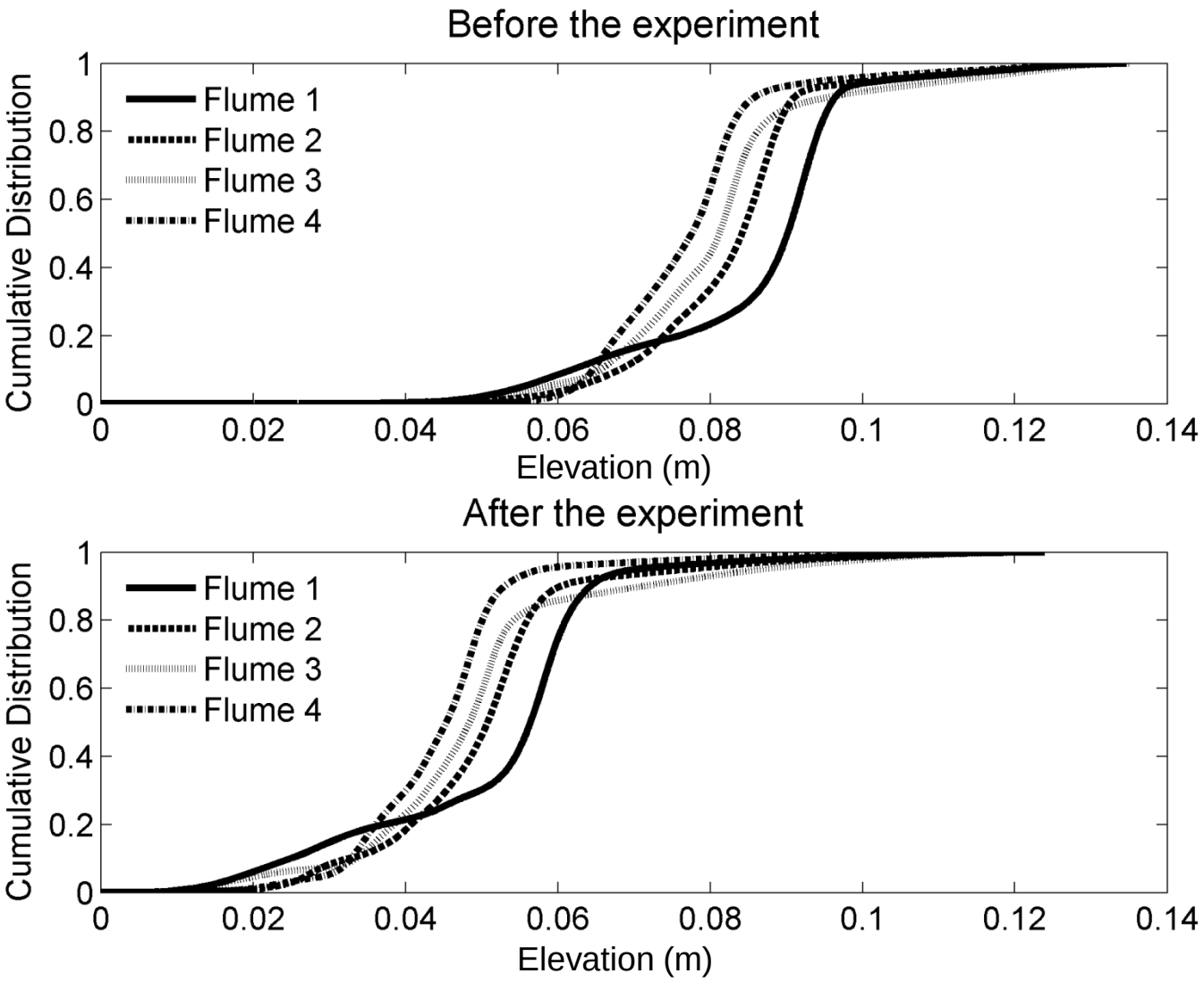
Before the experiment
Cumulative Distribution
Elevation (m)
Flume 1
Flume 2
Flume 3
Flume 4
0
0.2
0.4
0.6
0.8
1
0.02
0.04
0.06
0.08
0.1
0.12
0.14
After the experiment
Cumulative Distribution
Elevation (m)
Flume 1
Flume 2
Flume 3
Flume 4

Figure 11

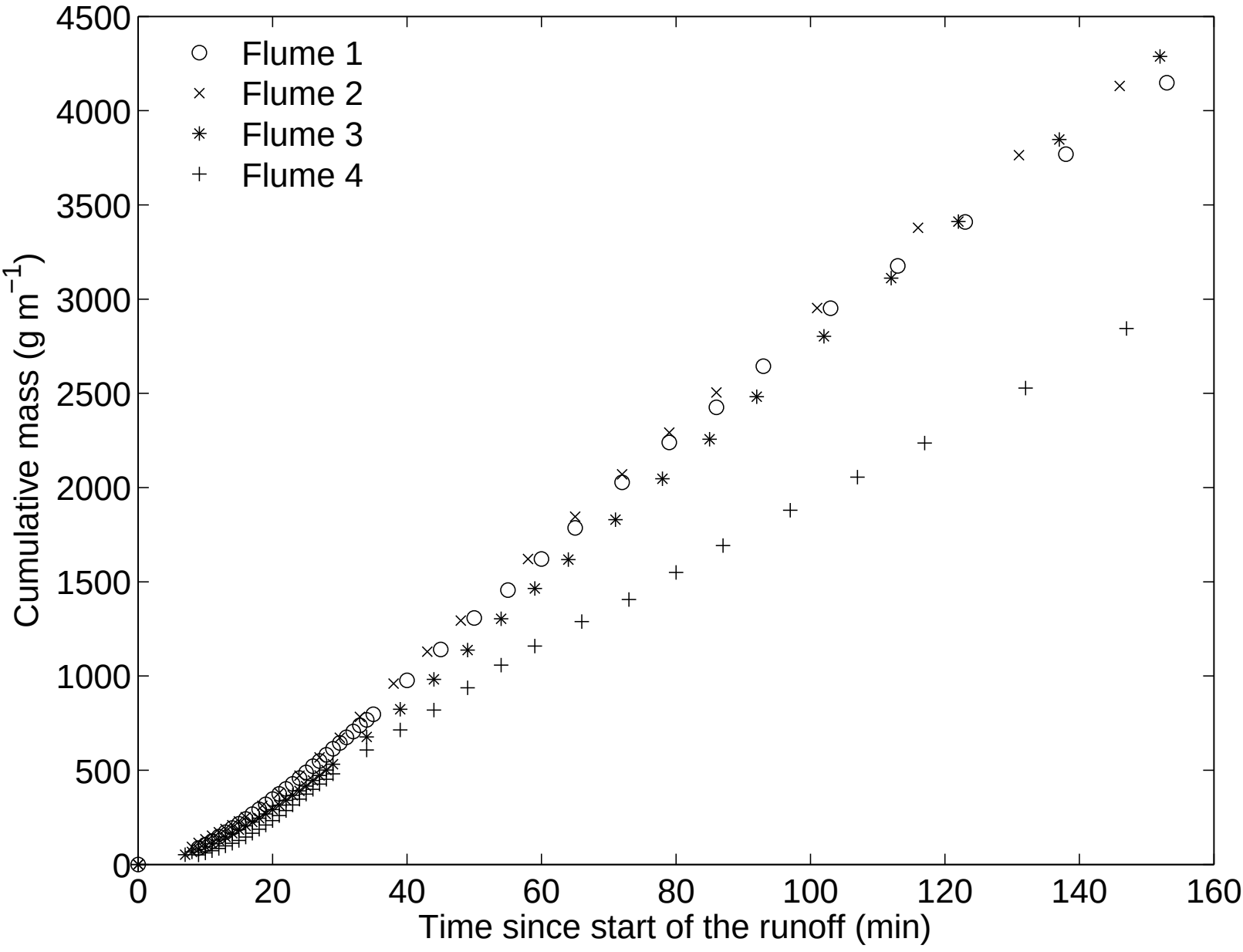
Flume 1
Flume 2
Flume 3
Flume 4
Cumulative mass (g m^{-1})
Time since start of the runoff (min)
0
500
1000
1500
2000
2500
3000
3500
4000
4500
0
20
40
60
80
100
120
140
160